15

Possibilities for Flexible MEMS: Take Display Systems as Examples

Cheng-Yao Lo
National Tsing Hua University
Taiwan (Republic of China)

1. Introduction

After the development of cathode ray tube (CRT) in the 19th century and the commercialization of television (TV) in the 1930s display devices are always one of the dream products in daily life. The revolutionary innovation from black-and-white to color display, from small size to large area, from curved surface to flat panel, and from space-consuming tube to short tube, all proved that the demands and distribution of display device was growing and played a critical role on civilization and industrialization.

Along the popularization of personal computer, the demand of CRT put the display technology and its industry to a highly growth field for the past few decades until the late 20th century. On the other hand, with the leaping progress of research and development on liquid crystal, liquid crystal display (LCD) also attracted customers' attention and overwhelmingly replaced CRT and suppressed CRT industry because of its light weight and thin body. Even though LCD's starting price was high, most of customers were still switching their display device from CRT since the bulky CRTs cost more when talking about office or house rent. Similarly to CRT, researchers also spent time developing thinner, lighter, wider viewing angle, shorter response time, and larger size LCDs. As a result, LCD became a main stream not only for computer displays, but also for recreation displays such as TV. In the same time, plasma display panel (PDP), and organic light emitting diode (OLED) also found their application fields as a flat panel display device to replace the role of CRT. Unfortunately, PDP's high resolution and fast response time come with low life time and high power dissipation. The original advantage of large size display was also gradually replaced by the up-to-date LCD produced from the 6th-8th generation glass substrate. Thus PDP market is now suppressed by LCD and PDP manufacturers are also reducing their production. Although OLED was proved to be display-capable, recently commercialized OLED's blue color degradation still limits its application on information display. Since the demand for larger display size, wider viewing angle, and smaller body size are still growing, projection display such as back projection TVs and overhead projectors are built in parallel. Back projection TV, owing to its bulky size and low resolution, had limited applications and disappeared from market rapidly; overhead projectors, even though still find their way in the early 21th century, it was neither portable nor long lasting. Thus, how to realize a light weight, small size, and large display area comes to one end – flexible display. When display device becomes flexible, it must be light weight and portable. It must

also be with compact size when folded or rolled, and must be supporting large area when unfolded or unrolled. Hence the first idea within its applications is focused on electronic paper (e-paper). With the arising of the attitude towards ecological friendliness, the demands of paper reduction also transfer to and stress on the development of flexible display as an e-paper. A successfully flexible display is thus expected to be bendable, portable, light weigh, low cost, durable, and even disposable. On the other hand, from the technology point of view, to manufacture a flexible display typically requires a flexible substrate such as polymer plastic material, which adds more complicated factors into traditional electronic device's production line.

From the process flow we understand that there are several disadvantages when use polymer plastic material as flexible substrate. For example, high temperature thin film deposition will cause material deformation since most polymers' glass transition temperatures (T_g); points or even melting point are below 200°C. Some polymer materials are also weak to chemical treatment or plasma bombardment which usually carries ultraviolet (UV) light. Thus, in order to successfully handle flexible substrate during production, a new process system should be set up. This process system is expected to take advantage of substrate's flexibility for variety and to avoid previously mentioned drawbacks on polymer materials. As discussed before, the flexible display has to support large display area thus a large substrate also introduces process difficulties in a production line. Take current semiconductor apparatus as an example, up to 12-inch circular substrate can be supported with lowest unit cost. However, a 12-inch diameter area cannot be called large area display. The latest 8th generation LCD apparatus which supports up to 2160×2460mm substrate size will be very helpful for large area display but its transportation is always a problem. To overcome these issues, traditional printing processes are taken into consideration because flexible polymer substrate is just like paper, which can be bent during process and can be produced continuously. Both the material flexibility and process continuity are positive factors for large area device realization.

1.1 Flexible display systems

1.1.1 Gyricon

Historically, the very first flexible display system was realized with "Gyricon" media by Sheridon and Berlovitz in 1977 and its conceptual cross-sectional view is illustrated in Figure 1. This kind of material contains black and white colored beads (balls) with averaged size of 100μm. Since different colors on the bead carry different charge polarity and the beads are enclosed in liquid, specific color can be directed to specific direction by outside electric field. This kind of system can perform either binary (black and white) data or gray scale reflective light. This system also mimics the printing process on papers by putting this Gyricon sheet into programmable electric field "printer". Unfortunately this project was closed in 2005 for not profitable reasons by Xerox. Some main advantages and disadvantages of electrophoretic system are listed below:

Advantage

1. The first demonstration of e-paper with little flexibility,
2. Supports A4 size,
3. Pattern is programmable by controller (computer),
4. Supports gray scale display.
5. Zero power consumption for static display.

Disadvantage
1. Coarse resolution,
2. Slow response time,
3. No full color,
4. Impure color,
5. High operation voltage.

Fig. 1. Schematic cross-sectional view of Gyricon system.

1.1.2 Electrophoretic display

Electrophoretic system inherited some basic concepts from Gyricon. As depicted in Figure 2, electrophoretic system further reduced the beads' sizes and increased their density. The main difference between electrophoretic beads and Gyricon beads is there's only one color on one electrophoretic bead. This change makes electrophoretic system possible to show higher resolution and contrast. Furthermore, since beads' sizes (approximately 1μm) are smaller than Gyricon's, gray scale display can be divided into finer details. Similar to Gyricon, an outside electric field plays the critical role on controlling the charged beads' movement in a liquid environment. But different from Gyricon, where beads have to rotate inside the liquid and stabilize after long time; the electrophoretic beads don't have to wait for stabilization since the beads are with only one color. This makes the electrophoretic system response faster than Gyricon. Likewise, electrophoretic system does not require any maintenance voltage after operation. Some main advantages and disadvantages of electrophoretic system are listed below:

Advantage
1. Finer resolution (compared to Gyricon),
2. Faster response time (compared to Gyricon),
3. More gray scale options,
4. Capable for mass production,

Disadvantage
1. Still slow response time (for human perception),
2. Too high operation voltage.

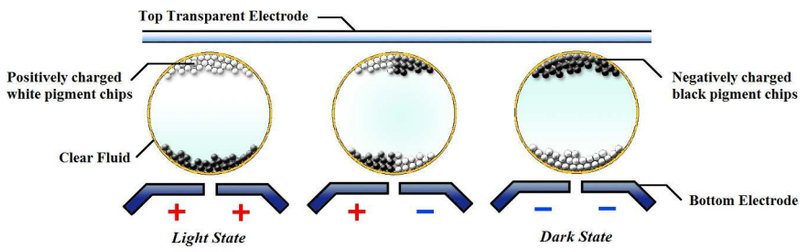

Fig. 2. Concept of electrophoretic system.

1.1.3 Electrowetting display

Compared to particle based Gyricon and electrophoretic display systems, electrowetting system uses all liquid material for color modification. This kind of concept takes advantage of Young-Lippmann's equation (Equation 1) to modify different surface energies between the droplet and the substrate underneath, which in turn changes the contact angle between the droplet and the substrate. Here, γ_{LG} is the surface tension between liquid and gas, γ_{SG} is the surface tension between solid and gas, γ_{SL} is the surface tension between solid and liquid, θ is the contact angle, V is the applied voltage, and C is the electric capacitance per unit area in the region of contact between a metal surface and the electrolyte drop.

$$\gamma_{LG}\cos\theta = \gamma_{SG} - \gamma_{SL} + \frac{CV^2}{2} \tag{1}$$

According to Equation 1 and Figure 3, the applied voltage will change the droplet's contact angle. A smaller contact angle represents a larger droplet diameter while a larger contact angle represents a smaller droplet diameter. By following this concept, an electrowetting display system was designed: The intermediate liquid was dyed for different colors while the water was kept transparent. Under normal (OFF) condition, the intermediate color liquid is laying under transparent water thus the reflective light shows intermediate liquid's color. Under operation (ON) condition, the intermediate color liquid is pressed into a specific corner of a pixel, leaving the rest area only with transparent water. Thus the reflection light with background color appears. By switching this system ON and OFF, two different colors can be switched for display purpose as shown in Figure 4. Since electrowetting system is using all liquid material for color modification, it is supposed to be flexible for display application. Some main advantages and disadvantages of electrowetting system are listed below:

Advantage

1. Gray scale is ideally controllable by applied voltage (contact angle),
2. Low cost,
3. Good color purity (not by mixing colors),
4. Can be designed for transmission or reflection type.

Disadvantage

1. Low resolution (limited by liquid suppressed at corners),
2. Low stability (gravity influence on liquid),
3. High power consumption (continuous power supply when ON).

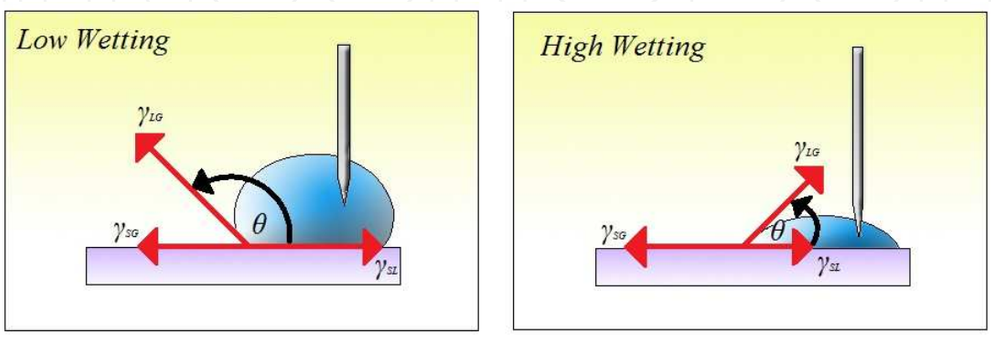

Fig. 3. Contact angle change by applied voltage is the basic of electrowetting.

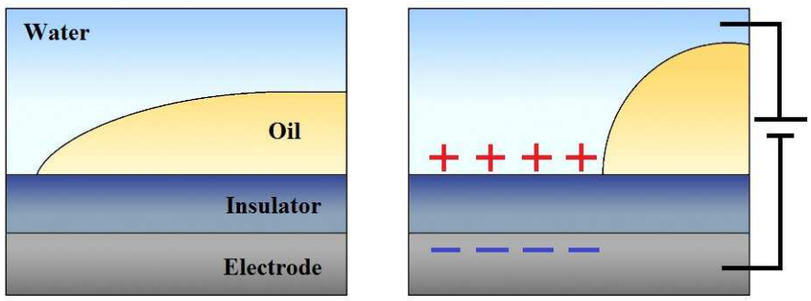

Fig. 4. Switching colors by controlling liquid's electrowetting performance.

1.1.4 Electrochromic display

Gyricon and electrophoretic systems are using physical control by electric field outside on colored particles and electrowetting system is also using physical control but the main material contains only liquid. Here, the electrochromic system is using chemical concept to change material's charging condition in dielectric electrolyte in order to change its light absorption band as shown in Figure 5. The electrochromic material can be either dissolved in the electrolyte or coated on the electrode substrate. Typical materials in electrochromic system are WO_3 and TiO_2. WO_3 had been reported with capability to change its colors between transparent under oxidation state and blue under reduction state; TiO_2 had been reported with capability to change its colors between transparent under reduction state and white under oxidation state. Thus, using only one electrochromic material can realize a two-color system and a combination of two electrochromic materials can realize a multiple color system. When the electrochromic material is thinly coated on the electrode, the whole structure will be bendable; when the electrochromic material is dissolved in electrolyte, the whole structure will also be bendable. Thus the electrochromic system can be used as a flexible color filtering device. Some main advantages and disadvantages of electrowetting system are listed below:

Advantage

1. Possible combinations for various colors,
2. Low operation voltage,
3. Can be designed for either transmissive or reflective.

Disadvantage

1. Low response time,
2. Color purity (depends on material's natural characteristic),
3. No black color.

All previous described technologies are supposed to be applicable on flexible substrate since all Gyricon, electrophoretic, electrowetting, and electrochromic (if material dissolves in electrolyte) are using liquid as intermediate or main material. But this also implies a reliability concern under critical operation conditions such as: high/low temperature, vibration or shock, and gravity influence, not mention to the jeopardy when the whole system is breaking and the chemical or electrolyte is leaking.

After reviewing these technologies from their basic operations, a summary can be made: Both physical and chemical concepts make the system slim and simple, thus the whole system can be fabricated on a thin substrate for flexible applications while reliability is a special concern. In contrary, stable, predictable, reliable, and reproducible mechanical

system is considered for flexible application. In which, electrostatic force controlled micro scale system with mechanical movement for color filtering is set to solve the reliability problem. With these settings, the structure becomes a micro electro mechanical system (MEMS).

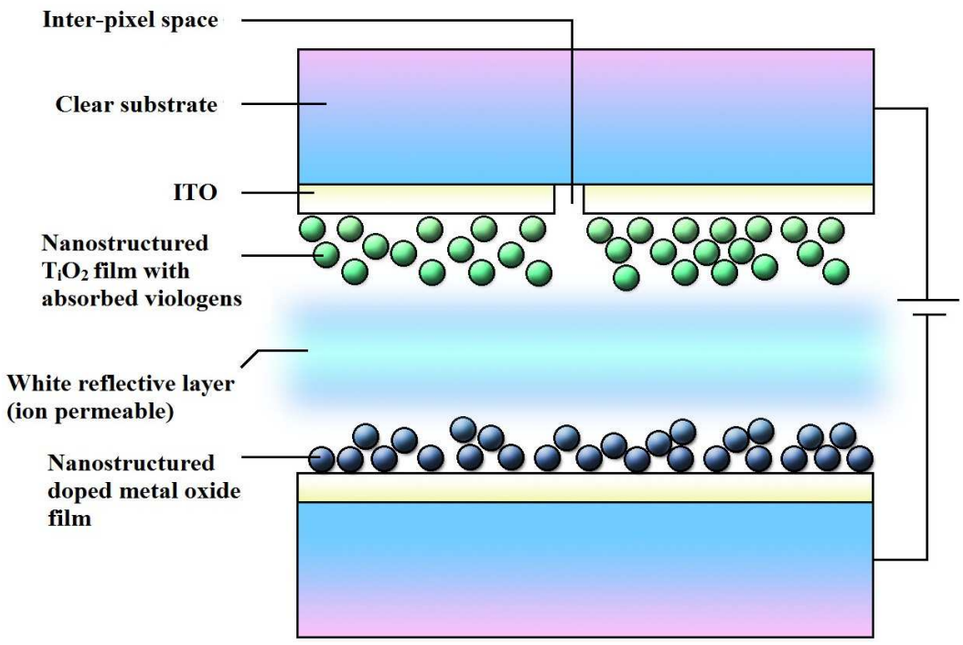

Fig. 5. The basic composition of an electrochromic system.

1.2 MEMS controlled display system

MEMS device is usually fabricated on solid substrate with batch photolithography process. In this section, some commercially realized MEMS display system will be discussed and reviewed by its color modification classifications.

1.2.1 Reflection

The most famous commercial reflective MEMS display system is Texas Instruments (TI) digital micromirror device (DMD). This device is fabricated on silicon (Si) substrate with complicated mechanical movement design. The key module – micromirror – is mounted on the center part of a torsion beam supported platform and the tilt angle of the platform can be controlled by electrostatic force to ±12°. With this setting, the reflection light from light source can be directed to display location (ON state, with color) or a shutter (OFF state, black). This is the realization of basic optical MEMS mirror design and people can generate three primary colors by implementing three DMD modules together or by using a color filter on a single DMD module.

1.2.2 Diffraction

When optical slits' sizes are well designed, optical diffraction takes place when light goes through the slits. Take white light as an example, different wavelength components diffract into different direction. Thus when viewing angle is fixed, different diffraction grating

designs generate different primary colors. Sony's (originally developed by Silicon Light Machines) grating light valve (GLV) is one of the applications. Its MEMS part lies on the control and movement of its thin periodical metal ribbons. The ribbons reflect incident light under OFF state and specific wavelength is diffracted into designed direction when electrostatic force is applied. The individual control off each ribbon makes the system with different diffraction spatial frequencies for different colors. This device is usually made with complementary metal oxide semiconductor (CMOS) process.

1.2.3 Switching

Shutter is one of the applications in MEMS field and most uses of shutters are on optical or display categories. Pixtronix's digital micro shutter (DMS) is the representative device. DMS is fabricated by photolithography process on solid substrate with a suspension beam on opposite sides. The mechanical movement of the shutter layer opens and closes the output light from below generated by white light source. Its full color presentation comes from ultra fast switch rate which allows >1000 colors per second and avoids video fragments and color breakups.

1.2.4 Interference

Color interference takes place when a light beam is interfered by itself. To achieve this, one can put a dielectric material in another intermediate as shown in Figure 6. A key point to generate self interference is to have both reflection and transmission light at each interface. For example, light goes through Interface 1 or Interface 2 will generate two waves: one transmission light and one reflection light. Interference happens when transmission light from Interface 1 (t_1) encounters reflection light from Interface 2 (r_2). As a result, both constructive and destructive interference lights are formed as output. The Fabry-Perot interference condition (Equation 2) describes the constructive (visible) light under certain criteria. This Equation implies that when the incident angle (θ) and index of refraction (n) are understood, the output interference wavelength (λ) can be determined by dielectric material's thickness (d). The index m in the equation means any positive integer. A multiple layer stack for Fabry-Perot interference is normally the basic design concept of wavelength filters for visible colors and invisible transmission applications . Qualcomm's interferometric modulator (iMOD) took this advantage and commercialized small scale, low power consumption, high contrast device for display application. As shown in Figure 7, the reflection light's wavelength is determined by the gap distance between the solid substrate and a deformable metal membrane. Its OFF states reflect three primary colors and its ON states interfere the output lights to invisible region to compose a full color display.

$$2nd = m\lambda \cos\theta_1 \tag{2}$$

Although most of these MEMS ideas require solid substrate and CMOS photolithography process, some of them already showed flexible system with soft substrate when explaining MEMS with generalized terms: A mechanical movement system controlled by electrostatic force in micrometer scale. The rest issues lie on how to process or manufacture such flexible system.

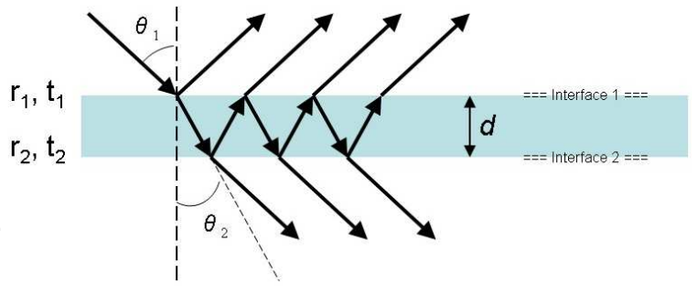

Fig. 6. A three-layer (two-interface) optical interferometer.

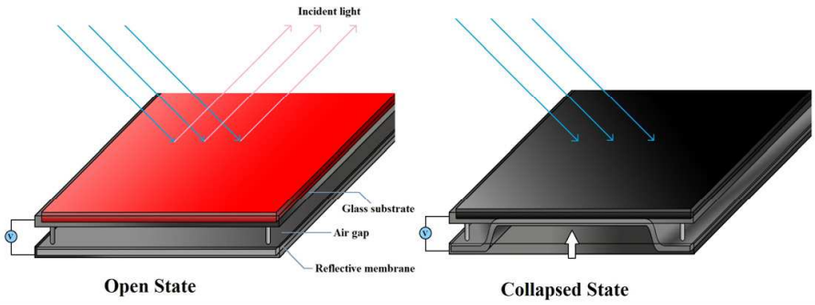

Fig. 7. A reflective Fabry-Perot interferometer iMOD.

1.3 Novel printing process system

Manufacturing technique for flexible electronic devices, especially for display devices, is the basic but also a crucial factor. As described and summarized previously, conventional CMOS photolithography techniques are not 100% applicable on polymer flexible substrates owing to heat, UV exposure, chemical treatment, and plasma bombardment. Thus, new process which is suitable for polymer substrate should be firstly developed to support the MEMS display system design. With polymer material's natural paper-like characteristic – stocks in a roll, conventional paper printing process seems workable for patterning the system's circuits as well as its structure. Here, some newly developed printing process will be introduced and evaluated to see how it can be modified and applied on a flexible polymer substrate based display system.

1.3.1 Gravure printing

After reviewing some trench patterning techniques, it is necessary to consider flat, continuous, and uniform layer stack. Within printing techniques, gravure printing is one of the most famous systems for ink printing on materials such as paper, plastic, and clothes. Its advantages are low cost, addable multiple inks, and gray scale. Its characteristic of low cost comes from the continuous mass production; its addable multiple colors comes from the combination of individual colors prepared by different cylinder to form a color mixture; its gray scale comes from the different designs of cell depth, cell density, cell angle, cell size, and cell shape. The cells are made by laser engraving and are recessed from the cylinder surface. A schematic plot of gravure printing in working is illustrate in Figure 8 and is usually used for continuous process. As shown in this figure, the ink cell on the cylinder represents how dense, how large, how high the printed patterns will be. Thus, gravure

printing is usually used for thick layer transfer. When ink's solid content is low (less sticky), printed high pattern density ink will spread and then merge together. This behavior provides a solution for continuous thick layer preparation.

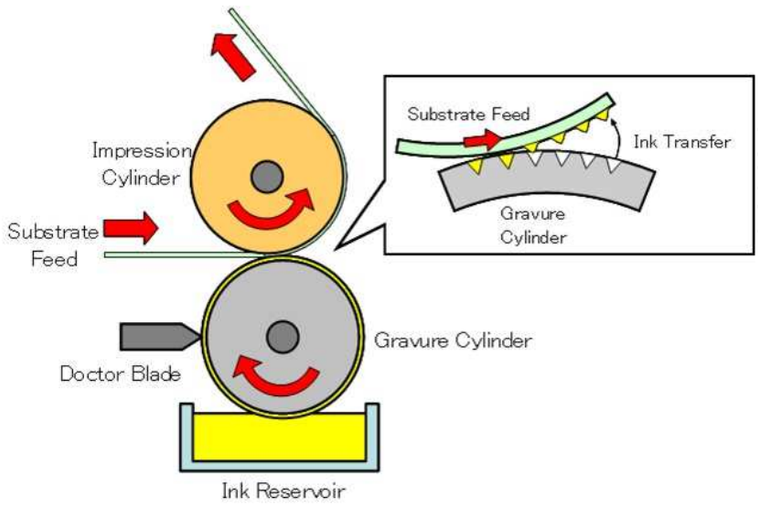

Fig. 8. An example of gravure printing system.

1.3.2 Flexography printing

Gravure printing is not possible to support thin layer deposition because in order to let printed inks merge, dense, deep, large ink cells are expected. Thus the transferred ink layer are usually ranging from 5-10μm. Flexography, as illustrated in Figure 9, uses a pattern plate to introduce ink from the anilox roller to the substrate. Since the patterns on the plate are

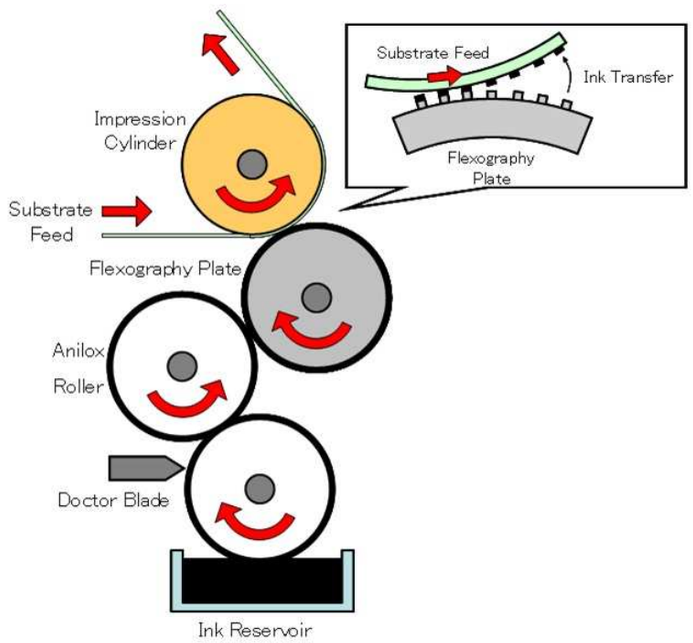

Fig. 9. An example of flexography printing system.

raised from the plate surface, the transferred ink amount depends only on the substrate's surface condition and ink's characteristic. However, flexography is suitable for thin layer (<2μm) deposition for good uniformity. There's also no ink rheology requirement generated from gravure printing's ink merge process. For pattern isolation, both hot embossing and laser ablation introduce fast and simple solutions but also bring some uniformity concerns. For layer deposition, even though gravure is used for thick layer and flexography is used for thin layer, how precise the thicknesses are seriously influence the optical design in a display device. But apparently, to perform integration process on a flexible substrate, the printing techniques described in this section are compulsory. Other printing techniques such as screen, inkjet, and offset are not suitable for this study but are widely discussed for flexible electronic devices' applications.

1.4 Target application

Section 1.1 already detail described why flexible display is necessary in the future and how those promising technologies are being realized and commercialized nowadays. The technologies introduced in section 1.1 have different target applications and markets and thus are with different concepts. It is obvious that no single technology can satisfy all requirements with all advantages such as low power consumption, high brightness, and fast response time. As a result, this chapter wants to cover and target at the large scale flexible display area for signage, advertisement, and decoration purpose. This means that this chapter is not necessarily pursuing a fine resolution, vivid true color, and fast response which are fundamental factors for TVs and monitors. Nevertheless, this study still looks for and tries to realize these good characteristics as reasonable as possible under some natural limitation such as availabilities of materials and configuration of apparatus. One of the most interesting examples of its applications for this study is to replace the mosaic windows which are usually decorated in churches as a motive. When the above targets are realized, the large scale flexible display sheet will be very distinguishable from previously mentioned flexible display systems and also those MEMS devices listed in section 1.2. Finally, this device will not only support uneven surfaces but will also be programmable to change the mosaic patterns without artificial backlight.

2. System design, material evaluation, mechanism, and simulation

Some flexible display ideas and control mechanism have been introduced. Within them, the Fabry-Perot was evaluated as the most promising system to be controlled by MEMS. This chapter then chose the MEMS as the flexible display's control system with Fabry-Perot color interference concept.

2.1 The Fabry-Perot interferometer

2.1.1 Mono layer model

The model in Figure 10 shows the basic composition of a Fabry-Perot interferometer. In the figure there are two intermediates which form two interfaces. When a light goes through the Intermediate 1 and reaches the Interface 1, a reflective light and a transmissive light will be generated at Interface 1. The transmissive part will again be divided into a reflective light and a transmissive light at Interface 2 when it goes through the Intermediate 2 and reaches the Interface 2. Likewise, a reflective light and a transmissive light will be generated at any

interface even though both the reflective light and the transmissive light decay in the intermediates.

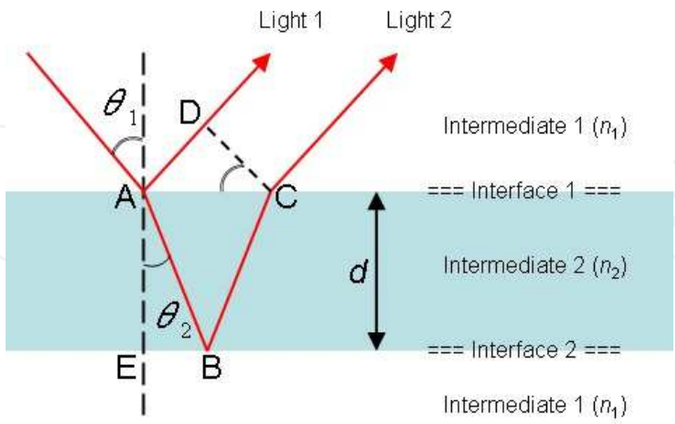

Fig. 10. A basic Fabry-Perot interferometer.

Color interference takes place when there is optical path length difference (Γ) between two or more light components traveling together. In this figure, the reflective Light 1 and the reflective Light 2 have optical path length difference Γ:

$$\Gamma = n_2(\overline{\mathrm{AB}} + \overline{\mathrm{BC}}) - n_1\overline{\mathrm{AD}} \tag{3}$$

Here, n_1 and n_2 is the index of refraction of Intermediate 1 and Intermediate 2, respectively. Since the angle of incidence equals to the angle of reflectance, which is θ_2 in Figure 10, thus,

$$\overline{\mathrm{AB}} = \overline{\mathrm{BC}} = \frac{d}{\cos\theta_2} \tag{4}$$

$$\begin{aligned} \overline{\mathrm{AD}} &= \overline{\mathrm{AC}}\sin\theta_1 \\ &= 2\overline{\mathrm{EB}}\sin\theta_1 \\ &= 2(\overline{\mathrm{AE}}\tan\theta_2)\sin\theta_1 \\ &= 2d\tan\theta_2\sin\theta_1 \end{aligned} \tag{5}$$

According to Snell's law:

$$n_1\sin\theta_1 = n_2\sin\theta_2 \tag{6}$$

The distance $\overline{\mathrm{AD}}$ becomes

$$\overline{\mathrm{AD}} = 2d\tan\theta_2\left(\frac{n_2}{n_1}\times\sin\theta_2\right) \tag{7}$$

Replace $\overline{\mathrm{AB}}$, $\overline{\mathrm{BC}}$, and $\overline{\mathrm{AD}}$ by Equation 4 and Equation 5 into Equation 3,

$$\Gamma = 2n_2 d \frac{1 - \frac{1}{n_1} \times \sin^2 \theta_2}{\cos \theta_2} \tag{8}$$

With trigonometric function:

$$\cos \theta_2 \tan \theta_2 = \sin \theta_2 \tag{9}$$

$$\cos^2 \theta_2 + \sin^2 \theta_2 = 1 \tag{10}$$

and take atmospheric air as Intermediate 1 with n_1=1, the optical path length difference becomes

$$\Gamma = 2n_2 d \cos \theta_2 \tag{11}$$

A constructive interference takes place when the two reflective lights are in-phase and a destructive interference takes place when the two reflective lights are out-of-phase. A maximum constructive interference happens when the two lights are with 0° phase difference or zero (or 2π) phase change:

$$2n_2 d \cos \theta_2 = m\lambda \tag{12}$$

Similarly, a minimum destructive interference happens when the two light are with 180° phase difference or π phase change:

$$2n_2 d \cos \theta_2 = (m - \frac{1}{2})\lambda \tag{13}$$

Here m is an integer and λ is the wavelength for both cases. The interference from the transmissive side can be also evaluated from the Interface 2.

2.1.2 Multiple layer model

Since the system is designed for information display, a maximum constructive interference is expected. According to Equation 12, one can easily design specific output light (wavelength) with specific intermediate (n_2, d) under fixed angle of incidence θ_2. It is also possible to calculate a multilayer system according to Equation 8 when the intermediate material is not air. Based on Figure 10, a multilayer structure shown in Figure 11 was chosen for color filtering. A premise is also made here: The color (color 1) filtered by the structure in Figure 11(a) is different from the color (color 2) filtered by the structure in Figure 11(b). The change of the multilayer structure hence lies on the mechanical control by MEMS. Here a special note should be put that a color of either color 1 or color 2 is not necessary to be both destructive interferences, rather, a color will be good enough to distinguish from another even though it is not formed by interference. The multilayer system in Figure 11 is switching between six layers and five layers (excluding ambient air layers: Intermediate 1). Thus, when talking about a multilayer system with more than three intermediates (four interfaces), the optical path length difference becomes relatively complicated which will be discussed and simulated by commercial software later.

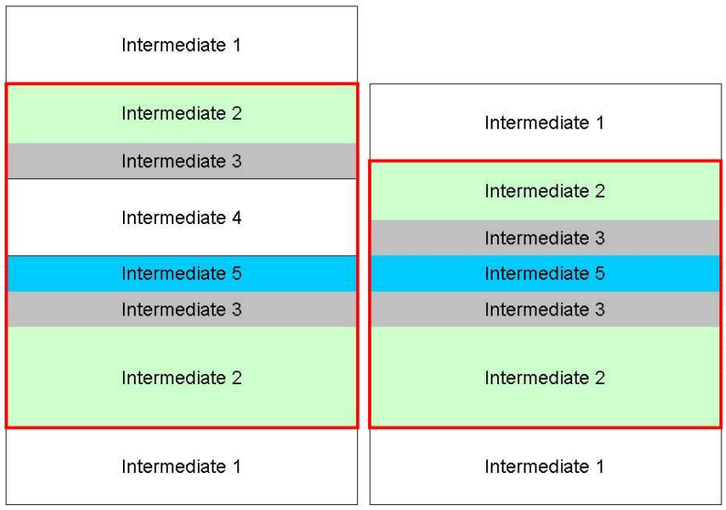

Fig. 11. The system design for two colors.

2.2 Color design and simulation

2.2.1 Color purity consideration

With the layer definition in Figure 11 and the Fabry-Perot interferometer concept, color designs in this section will help to decide how thick those layers should be and what kind of optical characteristics should they have for the three primary colors: red, green, and blue for full color applications. Previous report showed distinguishable yet poor colors especially for red. The root cause is the extra peak in blue region for red color, as a result a pink or purple color was shown. The author also implied a solution with new layer design which reduced the isolation layer's (Intermediate 5 in Figure 11) thickness from 370nm to 185nm. However, 185nm thickness was neither achieved nor disclosed. Besides the color purity issue, its transmittance for red, green, and blue was low and also not balanced. The unbalanced transmittance increased the design difficulty for backlight.

Within normally used metals, aluminum (Al) and copper (Cu) are widely used for their low cost and good conductivity while silver (Ag) and gold (Au) are also good but expensive. From the index of refraction (n) point of view, all Au, Al, and Cu show large difference under different wavelength. From the light wave phase (Φ) point of view,

$$\begin{aligned} \Phi &= \alpha \times x \\ &= \frac{2\pi}{\lambda} \times x \\ &= \frac{2\pi f}{n \times v_p} \times x \end{aligned} \tag{14}$$

where α is the wavenumber, x is the propagation distance, λ is the wavelength, n is the index of refraction, f is the frequence and v_p is the phase velocity. Thus the same input light with the same phase will generate two different phase output light owing to different index of refraction. According to this, a relatively uniform n value distribution for visible region (400-700nm) of a material is highly expected to solve the unbalanced intensity issue. Ag showed small n value difference across the visible region which suggests a structure change

solution: To replace Al by Ag for Intermediate 3 as electrodes in Figure 11. However, since the n value change and according to Equation 12, a suitable intermediate thickness (d) should also be evaluated.

2.2.2 Transmittance consideration

On the other hand, when trace the low transmittance with Al's optical parameters, a hint from its absorption coefficient (k) also emerges. Since k value means the decay behavior as well as how the light is absorbed in the intermediate, the higher k value is the lower the transmittance is. Al's k value ranges from 3.9 to 7 in visible region which is relatively higher when compared to Au, Ag, and Cu. We also understand that even Ag has higher k value in red and green region compared to Au and Cu, it is very suitable to replace Al to increase the transmittance for all red, green, and blue colors. Figure 12(a)-(c) and Figure 12(d)-(f) are the simulation results done by commercial software Optas-Film with structures of Figure 11(a) and Figure 11(b), respectively. The only variable in Figure 12(a)-(c) was the thickness of Intermediate 4 and the only variable in Figure 12(d)-(f) was the thickness of Intermediate 5 in Figure 11. The best condition for Intermediate 4's thickness was 600nm which shows a very distinguishable white color. With this setting, the best conditions of Intermediate 5's thickness are 160, 325, and 240nm for red, green, and blue, respectively. The transmittance in Figure 2-4 followed the optical design and thus proved higher transmittance with balanced output for all primary colors.

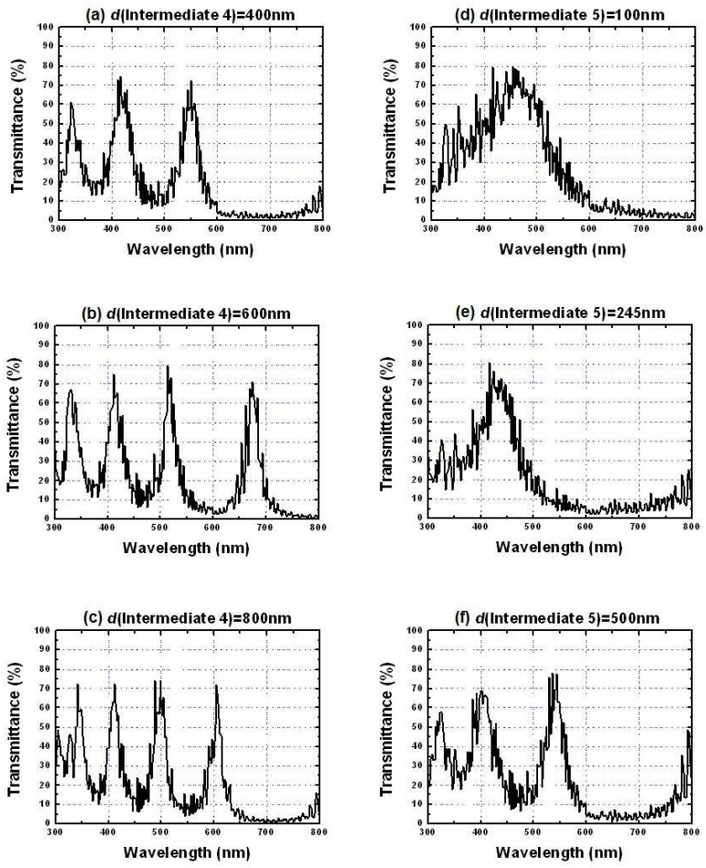

Fig. 12. Simulated transmittance with structures in Figure 11.

2.2.3 Color purity deviation

Without putting the output wavelength on a color chart it is very difficult to judge whether the output colors are vivid and pure or not; without quantifying the improvement it is very difficult to tell how good the new design is. Normally, the color purity is measured and illustrated on the CIE chromaticity diagram published in 1931 with (x, y) coordinate system or in 1976 with (u', v') coordinate system. The translation between these two systems follows the following formulas:

$$u' = \frac{4x}{-2x + 12y + 3}$$
$$v' = \frac{9y}{-2x + 12y + 3} \tag{15}$$

Here, only the CIE 1931 chromaticity system is used. Figure 13 is the color purity comparison of previous work, this design, and a CRT display. One can easily find that this work greatly pushed the green color to a better purity place while keeping the red and blue colors' purity similar. In order to quantify how much the improvement is, a color purity deviation (CPD) is firstly defined as the shortest distance between two points on the diagram with the following equation:

$$CPD = \sqrt{(x_T - x_{SE})^2 + (y_T - y_{SE})^2} \tag{16}$$

Here the subscript T means the target coordinate and the subscript SE means the simulated or experiment data coordinate. The best and the smallest CPD value are both 0 (zero). Based on the optical parameters analysis, the new design which inaugurated Ag as electrode material improved all the transmittance, balance between all colors, and the color purities. The incoming challenge thus lies on how to switch this Fabry-Perot interferometer system between the two states illustrated in Figure 11.

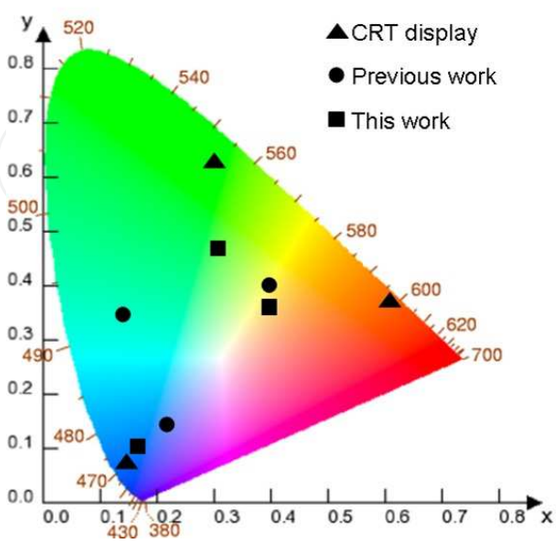

Fig. 13. Color purity distribution and the improvement comparison.

2.3 The MEMS model and simulation

A MEMS controlled system to switch a multilayer structure (Figure 11) of Fabry-Perot interferometer for different colors has been decided in previous section. Since the color design in section 2.2 already showed a very promising two-state color system, this section will handle how to design and prepare the structure in Figure 11 as a MEMS. Within all MEMS driving methods, the electrostatic way is believed to be suitable for structure in Figure 11 owing to the straightforward vertical movement. The structure in Figure 11 is also designed for electrostatic driving since the two Intermediate 3 materials can serve as the two parallel electrodes and the Intermediate 5 material can serve as the isolation layer when the two parallel parts are in contact.

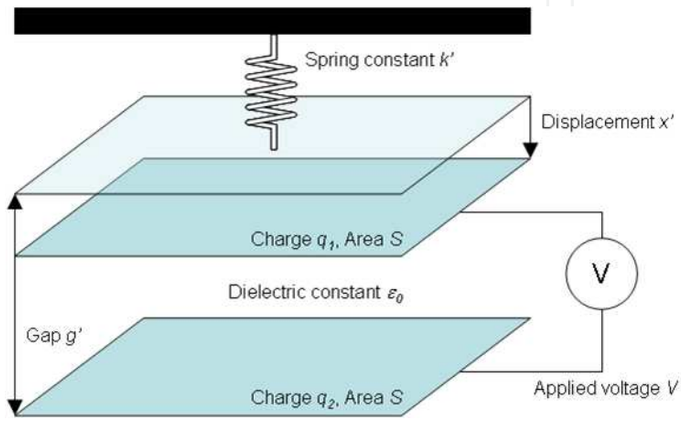

Fig.14. A parallel plate actuator system.

Suppose there are two particles in a space separated by distance g, a Coulomb (electrostatic) force F exists between these two charges:

$$F = k_C \frac{q_1 q_2}{g^2} \tag{17}$$

Here k_c is the Coulomb force constant whose value is $8.99\times10^9 \mathrm{Nm^2C^{-2}}$, and q_1, q_2 are the particle charges. A parallel plate system shown in Figure 14 consists two conductive layers and those layers are capable to stock charges. Charges can be supplied by outside source and the parallel plates start to attract with each other when the Coulomb force is strong enough. Thus, when two large plates are separated by spacer structure at the edges, its center part can be treated as a parallel plate system. A schematic plot is illustrated in Figure 15.

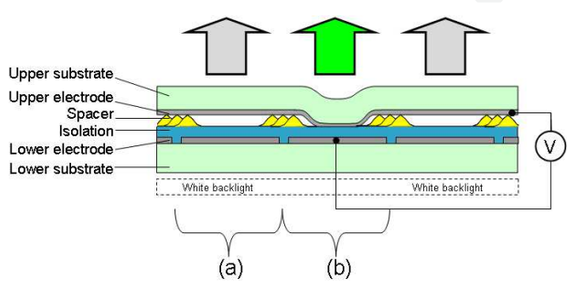

Fig. 15. The MEMS structure in (a) OFF state and (b) ON state.

2.3.1 Mathematical model

Even though the main part of Figure 15 can be expressed by a parallel plate, the whole structure still contains fixed ends close to spacer structures. A complex model combines these two parts is then necessary. The complex model of a single pixel (one parallel plate set) was divided into two parts horizontally and was further divided into two parts of a single-end fixed cantilever and a parallel plate as shown in Figure 16. The left part of Figure 16 is a cantilever which is fixed at one end and bending at another. The right part of Figure 16 is a parallel plate system which moves up (OFF state) and down (ON state) when applied with electrostatic force. Since the cantilever part is connected to the parallel plate part, when the plate moves down the cantilever is pulled down. When ON, the parallel plate system suffers an electrostatic force and tends to stay in contact while the cantilever suffers a reaction force and tends to return to the original (upper) position. In this model, the displacement x' in Figure 14 moved the entire gap g.

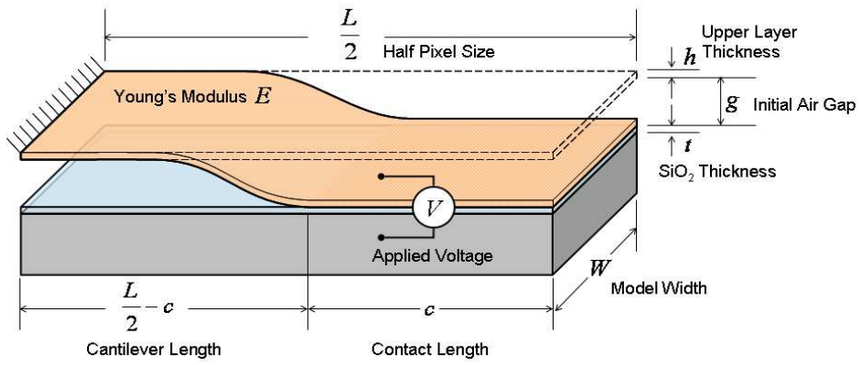

Fig. 16. The MEMS model from a half pixel of Figure 15(b).

The electrostatic force on the parallel plate system is:

$$F_p = \frac{1}{2}\varepsilon_0\varepsilon_r \frac{W \times c}{[(g+t)-g]^2} V^2 = \frac{1}{2}\varepsilon_0\varepsilon_r \frac{W \times c}{t^2} V^2 \tag{18}$$

The reaction force on the cantilever part is:

$$F_c = k' \times g = \frac{EWh^3}{4(\frac{L}{2}-c)^3} \times g \tag{19}$$

An overall stable system will be formed when these two force are in equal:

$$\frac{1}{2}\varepsilon_0\varepsilon_r \frac{W \times c}{[(g+t)-g]^2} V^2 = \frac{EWh^3}{4(\frac{L}{2}-c)^3} \times g \tag{20}$$

2.3.2 Simulation prediction

By rearranging Equation 20, a relationship between the contact length (c) and the applied voltage (V) can be set up. With this relationship, one can estimate the contact area and its

percentage under certain applied voltage. Similarly, one can also expect the operation voltage for specific contact area. The following simulations were performed under the following parameter settings: ε_0 = 8.85×10^{-12} A^{2}s^{4}kg^{-1}m^{-3}, ε_r = 3, h = 16μm, L = 2000μm, t = 0.3μm, E = 6.1GPa, and g = 0.6μm. Figure 17 is the simulation result with different pixel size (L). From these figures we understand that under the same applied voltage, a larger pixel will result in a larger contact area. From these figures we also understand that when one wants to achieve, for example, 90% contact area, a great operation voltage difference (55V for 1000μm pixel and 15V for 2000μm pixel) appears in Figure 17(a)-(b). Figure 17(c) is the simulation results with different spacer thickness (g). We understand that the operation voltage can be further reduced from 15V to 10V when change the spacer thickness from 600nm to 300nm. An examination in Figure 17(d) also indicated that when change the upper layer's thickness (h) from 16μm to 8μm, the operation voltage can be further reduced from 10V to 5V. Thus, a combination of these improvement designs, one can expect and design a low operation voltage device with this MEMS model. Other parameters concerning material characteristics such as ε_r and E, can also help on the operation voltage lowering but will not be considered here.

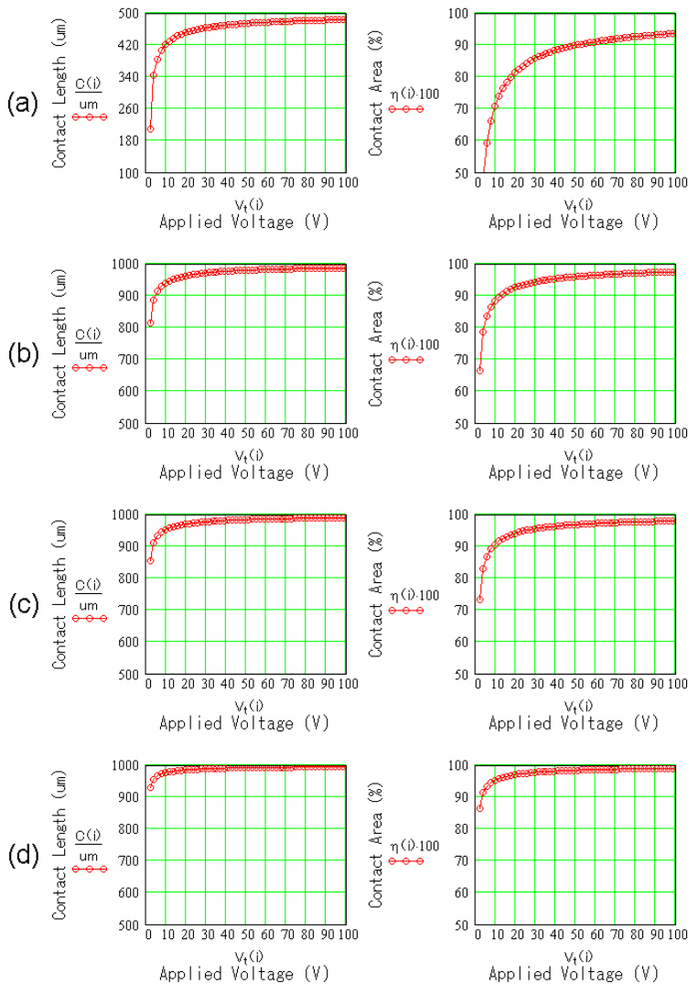

Fig. 17. Simulation results with different parameters from the MEMS model.

2.4 The horizontal structure design
2.4.1 Air pressure consideration

Until now, the device structure is designed and discussed vertically in detail thus its horizontal dimension and structure should also be considered. Previous report indicates high operation voltage with an enclosed Intermediate 4 in Figure 11 which is shown here in Figure 18(a) from its top. The author suggested some solutions to lower down the operation voltage such as to use thinner upper layer, to use thinner Intermediate 4, and to design a larger system. However, if the Intermediate 4 is trapped inside the system when ON, it will become a movement barrier or cause reliability issue unexpectedly. Since atmospheric air is designed for Intermediate 4, it is very possible to reduce the air pressure trapped inside the enclosed spacer area to alleviate the operation voltage. Figure 18(b) is the top view of a newly designed structure. Compared to Figure 18(a), the new design has some openings (air channel) on specific locations. These air channels serve as air evacuation paths when the device is ON. Figure 19 to Figure 21 are the simulations done with commercial software MEMSOne to explain how flexible can the air channel be designed and how the corresponding structure moves. Note that since there are design limitations on the structure by this software, the color legend means the areas in moving instead of its absolute displacement value. The value of opening ratio means the air evacuation efficiency while different designs imply different display shape because the air channel area can also be turned on if the opening ratio is large. Compared to the baseline design, we understand that increasing the opening ratio helps on enlarging the MEMS movement area. In the design of Figure 19, which represents the basic design in Figure 18 where the air channel was put in the center part of one spacer side, the displacement area increases when the opening ratio increases. The extreme model (Figure 19(c)) indicates that the displacement switched to the air channel area rather than the pixel area.

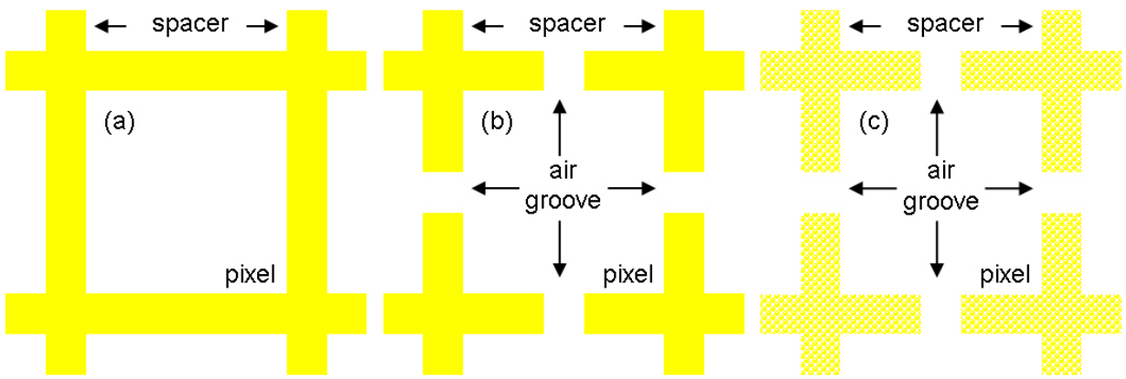

Fig. 18. Renewed spacer layer design's top views.

Similar effects also appeared on the Figure 20 designs, in which the air channel was divided into two sub-channels and were put at the both ends of one spacer side. One can find that up to 40% opening ratio, the displacement area follows the Figure 19 designs but the opening ratio of 60% (not shown here) and 80% (Figure 20(c)) ones helped the displacement continued to expand inside the pixel area. With this design improvement, we can positively change the unexpected displacement area caused by air channel to a reasonable and expectable area within the pixel. Based on Figure 20, the sub-channels were moved to the two ends of one spacer side and the spacer corners were also removed. The opening ratio of

one spacer side was thus still the same. The simulation result in Figure 21 did not change when the opening ratio is smaller than 20%, but interesting displacement took place at the spacer corners for opening ratio larger than 40%. This kind of motivation came from Figure 19(c), in which the displacement expanded to the direction with spacer's opening ratio large enough. Similarly, when the opening ratio in Figure 21(c) was large enough, the displacement area expanded to the corners when keeping its shape the same of a square. The structure design and simulation showed very promising results to realize the design in Figure 11.

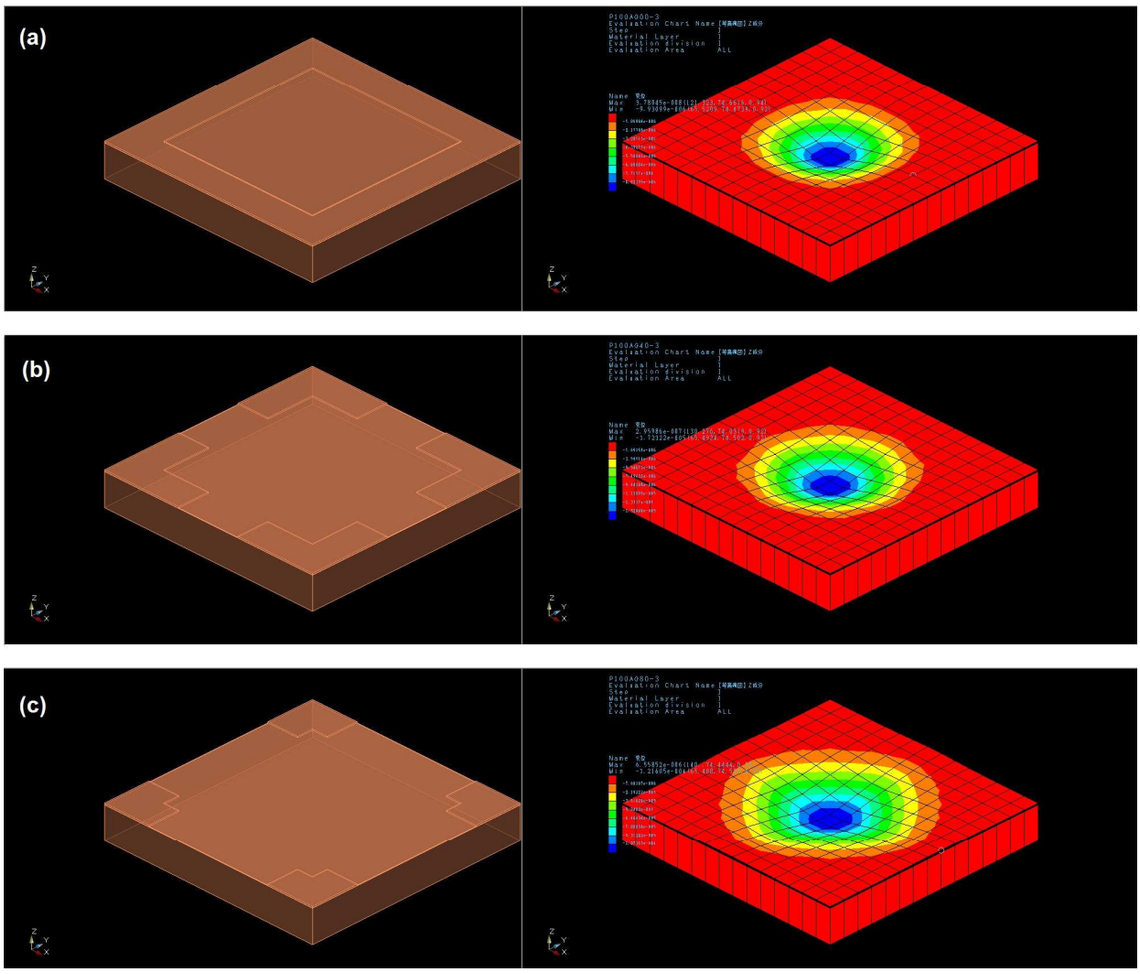

Fig. 19. Simulation results of opening ratio of (a) 0%, (b) 40%, (c) 80% for design 1.

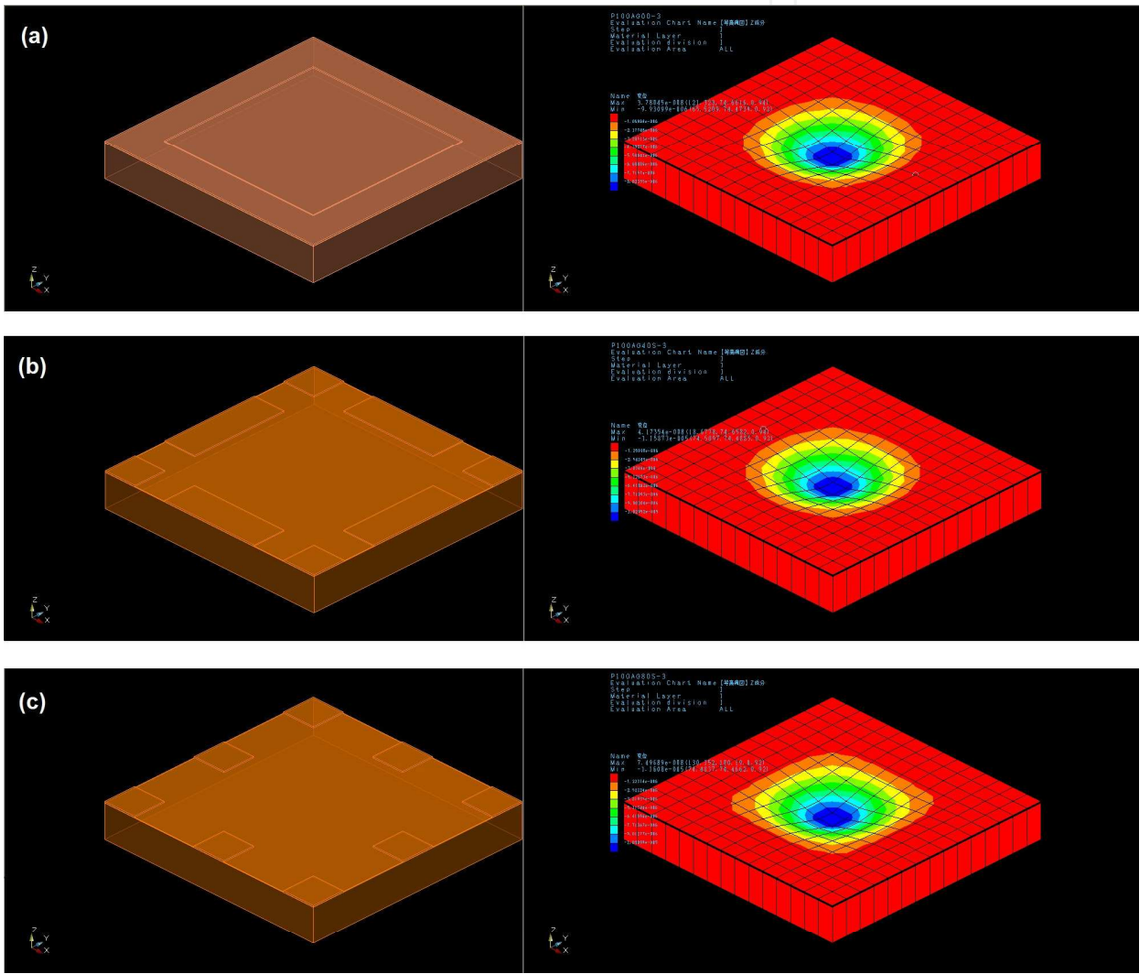

Fig. 20. Simulation results of opening ratio of (a) 0%, (b) 40%, (c) 80% for design 2.

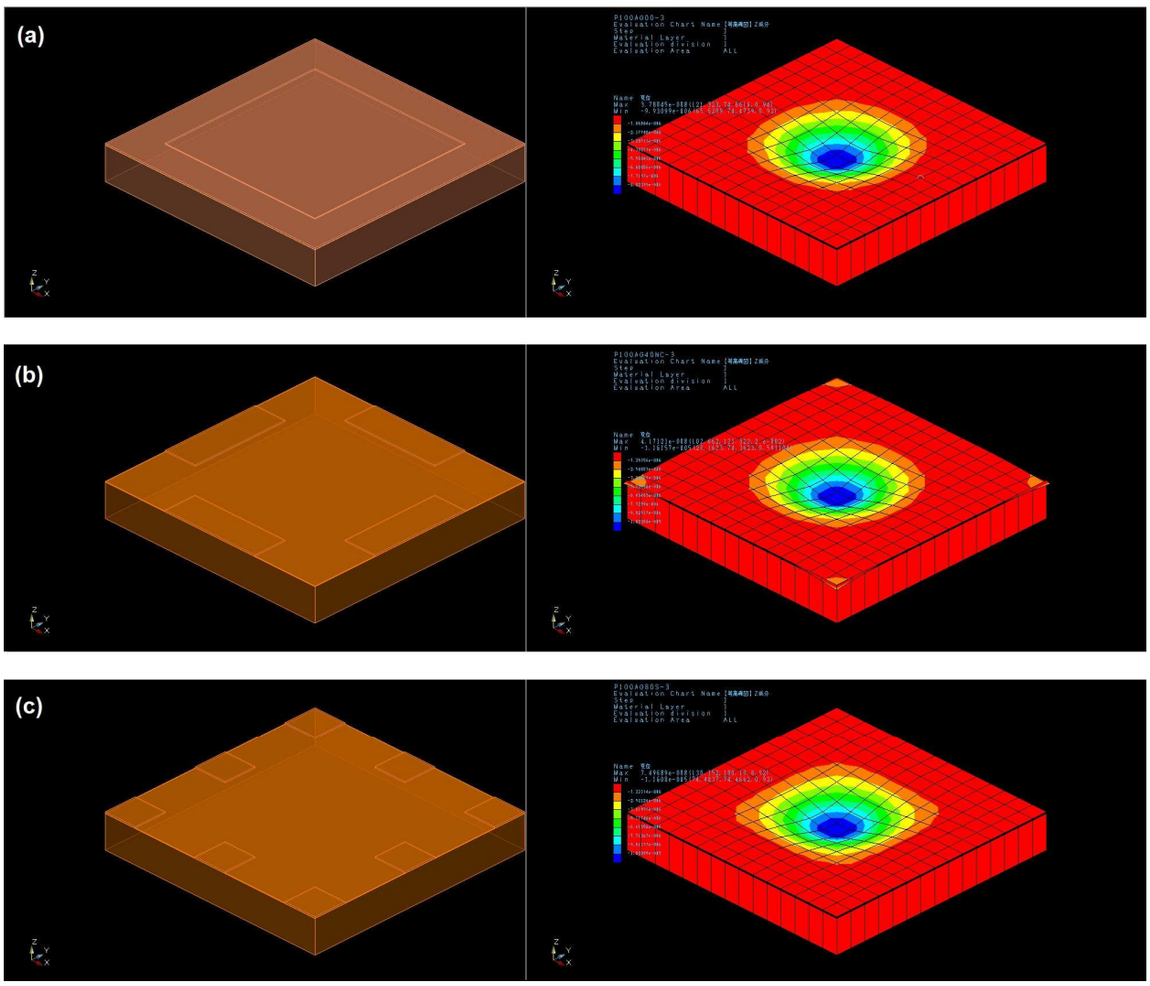

Fig. 21. Simulation results of opening ratio of (a) 0%, (b) 40%, (c) 80% for design 3.

3. Fabrication based on printing techniques

As introduced before, a novel process should be used for the special requirement on not only the structure's flexibility but also on the dot spacer layer design. Several promising solutions were examined in section 1.3 and with the structure set up before; material, process, and concerns will be discussed layer by layer here.

3.1 Material selection and system setup

3.1.1 Substrate

According to Figure 11, the whole structure will be made and the device will be operated in atmospheric ambient. Besides the Intermediate 1 in Figure 11, the multilayer structure contains six layers. The substrate material plays a crucial role for flexibility since it is the thickest part of the structure. When its thickness is below 500μm, it is with sufficient flexibility for display applications. However, when a large curvature is expected, only thinner substrates can satisfy this requirement. The latest glass manufacturing techniques support 30μm thick commercial products for large scale (300×400mm). Even though thin glass substrates provide very

promising options for curved or flexible applications with large curvature, its fragility still limits its realization on flexible electronic devices especially for portable products. The potential safety and reliability concerns also put a barrier between its benefit and realization. In contrary to the fragile glass, elastic polymer material (plastic) is a very good option for the substrate. Because the plastic substrate will be used for the flexible display system, some special requirements including:

1. Flexibility – Low Young's modulus (E) is highly expected,
2. Transparency – High transmittance in visible region (400-700nm) is necessary,
3. Cutoff – Unexpected wavelength (<400nm and >700nm) should be screened out,
4. Stability – Should be thermally and electrically stable,
5. Reliability – Have to be highly moisture, gas, and chemical resistive,

are primary material selection principles. Within polymer materials, one can screen out polyvinyl chloride (PVC), polycarbonate (PC), polyethylene (PE), and polyimide (PI) from stability, reliability, deformation, and transparency point of view, respectively. With these concerns, polyethylene teraphthalate (PET) and polyethylene naphthalate (PEN) are relatively suitable for this flexible MEMS design. PET is also famous for its low cost and high transmittance in visible region while PEN is famous for its high temperature stability and sharp cutoff performance for UV light. According to these characteristics, PEN was chosen as the substrate material.

3.1.2 Process environment for plastic substrates

Besides embossing and laser ablation, which are patterning techniques for isolation instead of layer stack, the other printing methods are all printing process related ideas. However, within the printing process ideas, the screen printing and ink jet printing are batch processes which do not provide any help on improving the low throughput in photolithography. A compromise between resolution and throughput results in the flexography and gravure printing. Their working concepts have been explained in section 1.3 and the detail process parameters and system specifications will be discussed in the following sections.

3.1.3 Ink

In printing process, ink plays a very important role. Refer to Figure 11, four layers should be processed besides plastic substrates. Within these four layers, two electrodes are Ag; and the isolation is SiO_2. Since the two substrates have to be laminated after process, the spacer should also cover the lamination job. A commercial standard spin-on SiO_2 (TOK, OCD T7-12000-T) was chosen for isolation. This material is composed of $RnSi(OH)_{4-n}$ and additives (diffusion dopants, glass matter forming agent, and organic binder) dissolved in organic solvents (ester, ketone, and mainly consisting of alcohol) in liquid form and thus is suitable for printing process. Its SiO_2 solid content is 12wt% and its thickness can be controlled by curing temperature, time, and spin speed if prepared by spin-on process. Because the roll-to-roll (reel-to-reel, R2R) system uses gravure printing, whose printing thickness can be adjusted by cylinder cell design, only the curing temperature and time were studied for the thickness control. Figure 22 is the thickness change after thermal and UV treatment which are two optional steps in the process system. Curing temperature was controlled between 100-150°C for less than 30min in this study. After the thermal treatment a 2min 12.5mW/cm^2 UV exposure was applied. The thickness change was mainly because the evaporation of solvent and the thickness is basically inversely related to temperature and

time. Since the R2R system is designed for high volume production and the plastic substrate is with low operation temperature limit, the data point of 140°C for 1min was set as the process variation boundary. On the other hand, since the spacer has to be sticky but does not have to be precise for physical and optical requirements, commercial adhesive glue (Herberts, EPS71) mixed with 35wt% hardener (Herberts, KN75) was chosen as the spacer material.

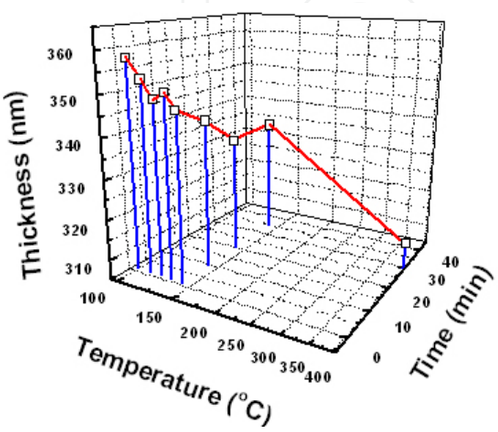

Fig. 22. Spin-on SiO_2 thickness variation after thermal treatment.

3.1.4 The roll-to-roll system

The final production system setup is illustrated in Figure 23. The flexible substrate is unwound from a roll and is then transferred into several different process steps. These

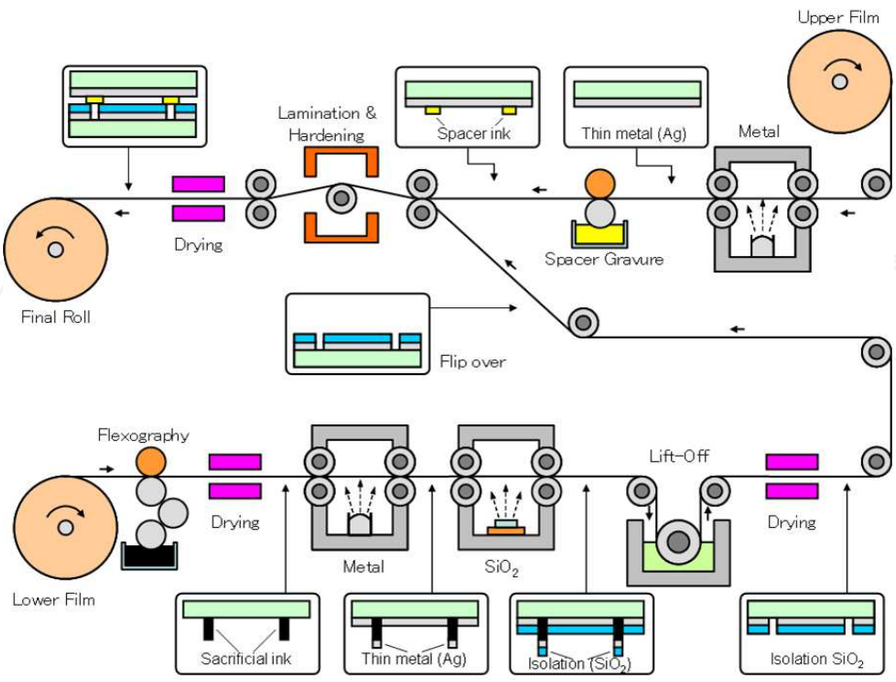

Fig. 23. Setup of the roll-to-roll process system.

process steps contain not only previously mentioned flexography and gravure printing but also conventional sputtering, cleaning, and drying/heating units. In the same time another or more substrate rolls can also be processed with similar sequences to form required patterns and layer stacks. These processed substrates might be finally laminated together and rewound back into a roll to complete this "roll-to-roll" process concept. Of course the final products can also be cut into sheets as a "roll-to-sheet" system. Note that even there is no multilayer combination and lamination process, the single substrate process is still a roll-to-roll system with roll-to-sheet capability. Before the whole continuous system is set up, individual parts in Figure 23 will be evaluated and single process step will be developed firstly with discrete units in the following sections.

3.2 Flexography printing

The concept of flexography printing was described in section 1.3. As mentioned previously, the flexography plate contains patterns raised from the surface and introduces very little ink from an anilox instead of the ink tank. Besides the adhesion force between flexography plate and ink, the plate merely plays a crucial role for ink transferring. Unfortunately, no commercial Ag ink can satisfy the specs and thus the direct pattern printing by flexography became inapplicable. A drawback of flexography printing laid on the uneven printed surface. The printed surface uniformity depends on a compromise between pattern integrity (contrast) and flatness: high pattern integrity requires thick (high solid content) ink, which in turn leaves peaks and valleys on the printed surface. Another drawback is that the printing process (not only limited to flexography) is highly direction oriented system: the pattern integrity is better along the printing direction (machine direction, mechanical direction, MD). Figure 24 is a printed example that along the printing direction more complete test lines are available. One can make modifications on ink quality and printing speed but can relatively induce worse surface uniformity and lower throughput unexpectedly. This printing behavior implies that one should design finer resolution along the printing direction to avoid broken lines. The process speed of Figure 24 was set to be 5m/min and its technique of lift-off will be explained in the next section. However, the drawback of surface uniformity is also just the merit of PR in photolithography: the rough surface provides good chemical resolving path during PR removal. With this advantage, a photolithography-like lift-off process was developed based on flexography printing.

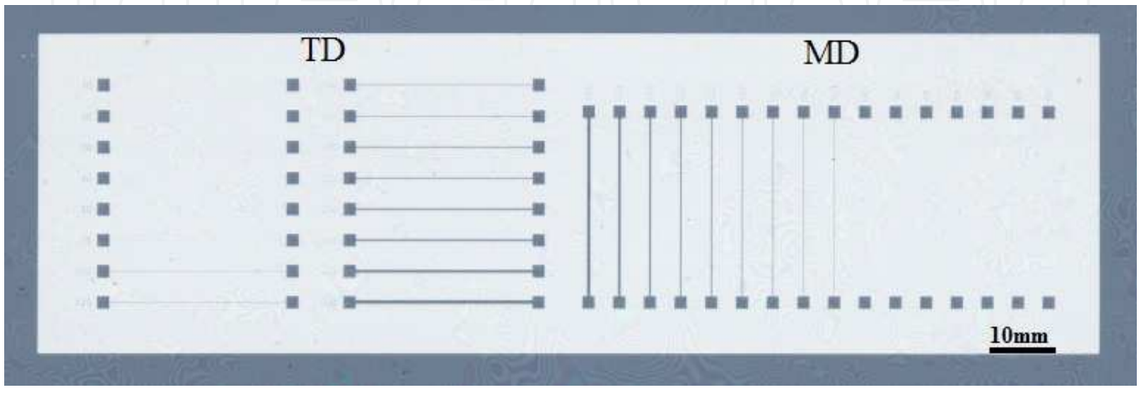

Fig. 24. Printing direction is with better resolution thus horizontal lines are thinner.

3.3 Lift-off

PR is recognized to be a patterning mask which influences the final structure on the substrates. With the uneven property of flexography printed surface, the ink was also treated as a sacrificial layer which provides protections on the substrate for layer stacking in the same figure. Here we modified Figure 23 from destructive process to constructive process for the same comparison basis. One can easily find that a process step of PR (ink) coating was omitted – the sacrificial pattern was directly printed from flexography plate while the photolithography exposed UV light through a photo mask. Similar to photolithography, this lift-off process is also a multilayer capable step as long as the sacrificial layer is thicker than the total thickness of multilayer. Figure 25 is a step-by-step example of lift-off process substrate. The thickness of sacrificial layer was ranging from 1-2μm which was higher and sufficient for multilayer stack with total thickness less than 1μm. The Ag sputtering was controlled with 20nm according to the color interference design in section 2.2. The third and the last step for the lift-off process is the sacrificial layer removal. In corresponding to the ink composition, basic chemicals such as acetone and ethyl acetate are suitable to dissolve it. It was also obvious that the substrate was flexible and was capable for large curvature process at this step. With ultra sonic vibration's help, the sacrificial ink dissolved in acetone in only seconds. Another important factor of heat influence on the removal efficiency was also carried out because of the drying unit after the sacrificial ink flexography printing. Here the sputter process influence was omitted because it was controlled under 60°C.

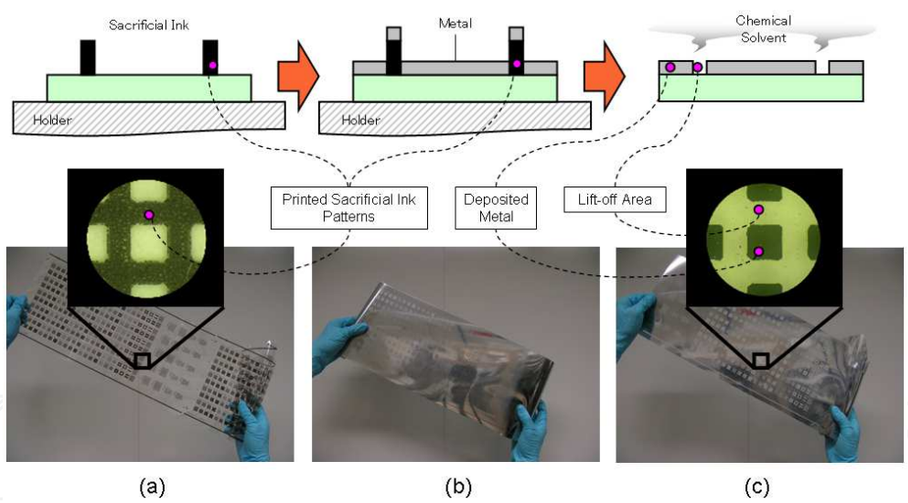

Fig. 25. Printing process is simpler than photolithography on step numbers: (a) sacrificial ink printing, (b) metal layer coating, and (c) sacrificial layer removal. The dimension of the square pattern in (a) and (b) is designed as 2000μm.

3.4 Gravure printing

The main difference between flexography printing and gravure printing lies on the controllability of printed layer. As shown in Figure 8 to Figure 9 and experimental results in section 3.2, it is apparent that the printed layer thickness and surface uniformity by flexography is merely controllable. The only solution for thick layer patterning is to choose from screen printing, ink jet printing, and gravure printing. The screen printing was

screened out in section 3.1 for its low process speed and batch production characteristic. From the ink engineering point of view, ink jet printing and gravure printing provide similar ink droplet behavior on the substrate but the control variety of ink jet printing is less yet it is also a kind of batch process. When thoroughly review the cell design of a gravure cylinder in Figure 26, one can easily find its control varieties such as: cell width, wall width, channel width, channel depth, cell density, screen angle, depth, and stylus angle. All these factors' combination results in a final parameter of volume. Table 1 is a list of designed patterns for different printed thickness as well as wetting performance. The adjustable parameters are the printing speed, the pressure force, and the contact angle between the doctor blade and the cylinder.

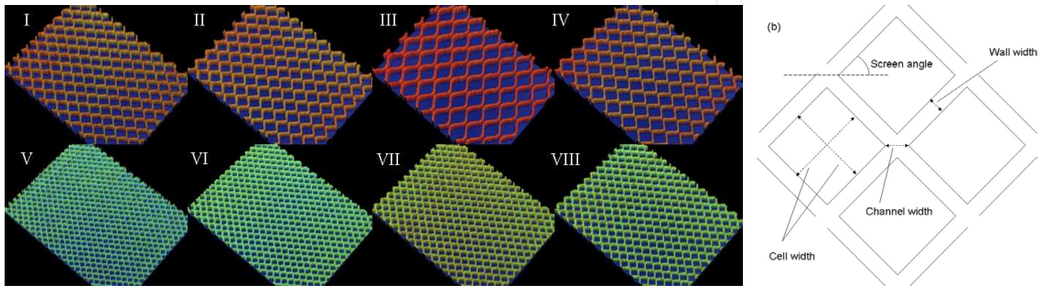

Fig. 26. A cell design set on the gravure cylinder and parameter definitions.

Design	I	II	III	IV	V	VI	VII	VIII
Mesh (line/cm)	60.8	53.8	41	47.8	116.4	104.3	89.9	80.9
Cell width (μm)	152	167.5	232.1	197.6	78.8	91.1	103.4	114.8
Wall width (μm)	12.6	18.3	11.7	11.7	7.1	4.8	7.8	8.8
Channel width (μm)	24	41	47	35	9	19	24	28
Channel depth (μm)	3.5	7.4	8.3	9.5	2	0	4.5	4.8
Cell density (%)	85.3	81.3	90.6	89.1	84.2	90.2	86.5	86.3
Cell depth (μm)	53.1	51.7	42.5	53	52.6	53.6	52.8	53.1
Screen angle(°)	56.9	60.8	58.6	59.4	31	34.4	39.1	43.5
Stylus angle (°)	121.5	119.8	129.8	130.1	119.1	118	118.7	118.3

Table 1. Detail list of cell designs.

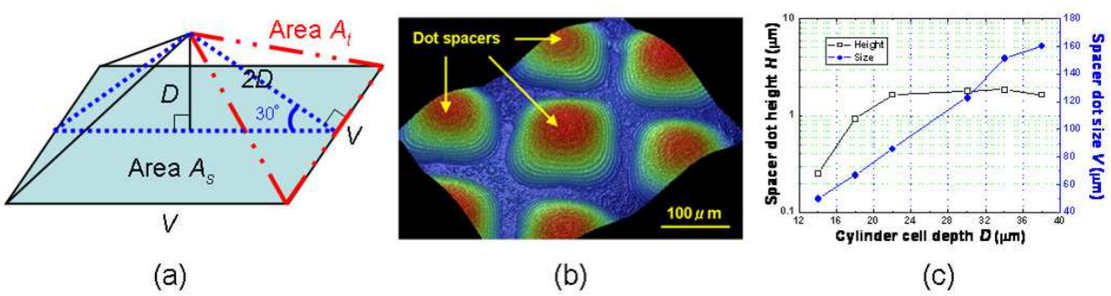

Fig. 27. (a) Cell model, (b) printed structures, and (c) relationship between (a) and (b) of gravure printing.

Figure 27(a) is a schematic plot for a single cell on the cylinder, the pyramid structure was laser engraved from the stainless steel cylinder. Figure 27(b) is the three dimensional printed structures measured optically and Figure 27(c) is an experimental plot for the printed pattern's size and its height. The interesting experiment result falls on that the printed pattern's size is linearly positively related to its designed dimension but the printed pattern's height is only in small range positively related to its designed dimension and finally trends to a saturation behavior. To explain this, the pyramid model in Figure 27(a) is used: The ink transfer process is a balance of force competition between the interface between the substrate (F_{is}) and the ink and the interface between the ink and the cell wall (F_{ic}). When F_{is} is larger than F_{ic}, the ink will tend to adhere to the substrate based on a premise that the ink quality is uniform within the whole droplet. Inversely, the ink will tend to stay inside the cell. With the relationship between the cell width (V) and the cell depth (D), angle γ can be calculated:

$$\gamma = \tan^{-1}(\frac{2D}{V}) \tag{21}$$

The stylus angle is approximately 120° and the total area (A_c) of four cell walls (A_t) is:

$$\begin{aligned} A_C &= 4A_t \\ &= 4VD \end{aligned} \tag{22}$$

Since the angle γ is 30°, the relationship between V and D is:

$$V = 2\sqrt{3}D \tag{23}$$

When replace V in Equation 22 with Equation 23:

$$\begin{aligned} A_C &= 4A_t \\ &= 8\sqrt{3}D^2 \end{aligned} \tag{24}$$

It is also obvious that the area of the opening area of the cell (A_s) is:

$$\begin{aligned} A_S &= V^2 \\ &= 12D^2 \end{aligned} \tag{25}$$

A comparison of A_c and A_s indicates that the difference of adhesion force becomes larger and larger when increasing the cell volume. As a result, the transfer of ink from the cell to the substrate becomes more and more difficult and final reaches its limitation. This special behavior will be alleviated if design the stylus angle to a larger value and the linear region can be extended. In order to keep the spacer dot height (H) – cylinder cell depth (D) curve linear, a critical angle γ_c , from Equation 21, can be calculated based on A_c=A_s or V=4D:

$$\begin{aligned} \gamma_C &= \tan^{-1}(\frac{2D}{V}) \\ &= \tan^{-1}(\frac{1}{2}) \\ &= 26.6^\circ \end{aligned} \tag{26}$$

When the angle γ is controlled smaller than γ_c, the adhesion force F_{is} and F_{ic} are at least balanced thus the transferred ink amount will be in linear relationship with the cell volume. For the structure design, the desired thicknesses fall in the linear region in Figure 27(c), thus the stylus angle of 120° was used. Experimented results shows that bigger and denser cell designs helped the printed ink to spread and merge (wetting). Further study and optimization should be done after this work for flatter surface. The final gravure printing process parameters for the isolation layer is summarized in Table 2. The best resolution of gravure printing was 200μm.

Target	Cylinder design (Table 1)	Pressure (N)	Speed (m/min)	Contact angle between doctor blade and cylinder (°)
Red (160nm)	V	550	32	60
Green (325nm)	VII			
Blue (245nm)	VI			

Table 2. The process parameters for different SiO_2 targets.

3.5 Lamination and finishing

After the process for both substrates in Figure 23 separately but before their lamination, one more study was performed to improve the MEMS flexible display device's contrast. Previous study only targeted on the demonstration of a single display pixel and did not address much on the overall performance of combined performance. A final compromise was made for the adhesive ink: a 35wt% glue solid content with 30wt% tiny black pigment (Sun Chemical, 049-72784) to block the transmission light from spacer areas. The lamination process was performed manually right after the spacer printing process. A final drying process was also applied right after the lamination step under 120°C for 1h to remove the extra solvent from the inks to reduce the reliability risks. The continuous substrate processed by roll-to-roll facility will be rewound back into a roll for stock and transfer before cut out into pieces for applications but the small area demonstrators fabricated by discrete tools discussed in these sections will be used for test in the next part.

4. Characterization and analysis

The discrete roll-to-roll printing system was used to check the printing capability, to characterize ink properties, and to study the system design. From system's point of view the continuous roll-to-roll printing processes handled the large area substrate before it was cut into small pieces for discrete roll-to-roll printing processes. From automation's point of view both the continuous and discrete roll-to-roll printing processes were automatically performed but the lamination process was semi-auto for alignment. The final production result of this study was not influenced by any factor of the system or the automation settings. Figure 28 is the pictures for the final demonstrators of (a) 3×3 active matrix array and (b) 21×39 passive matrix array. The 3×3 active matrix array device was examined and evaluated for various characteristics.

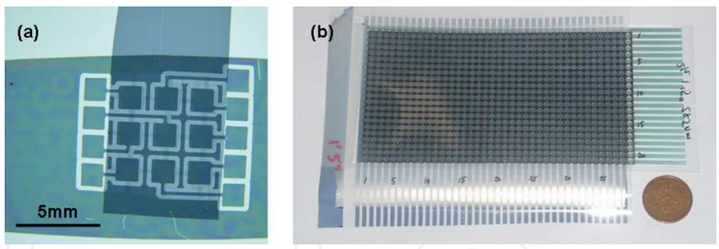

Fig. 28. (a) 3×3 active-matrix and (b) 21×39 passive-matrix demonstrators.

4.1 Optical performance

4.1.1 Color purity

The color purity simulation was done in section 2.2. The main influencing factor for color purity was explained in the same section by the control of metal electrodes. The best performance was concluded with 20nm Ag for its relatively balanced n value and relatively smaller k value. The color purity in CIE 1931 chromaticity diagram was measured by color tester (Yokogawa Denki, 3298F) with (x, y) axis system. A luminescent light (5500k) was used as the backlight. Figure 29(d) is the real performance of Ag electrode devices. The results typically followed the simulations and purer colors can be expected. From the datasheet PEN shows the best cutoff in UV region. Since strong UV light is harmful to human eyes and this MEMS display device claims sunlight as the backlight, a suitable substrate like PEN helps a lot on the UV cut out performance. When considering the visible region (400-700nm) in Figure 29(d), one can easily understand that only a single main peak appears in one color design which advanced each color's purity.

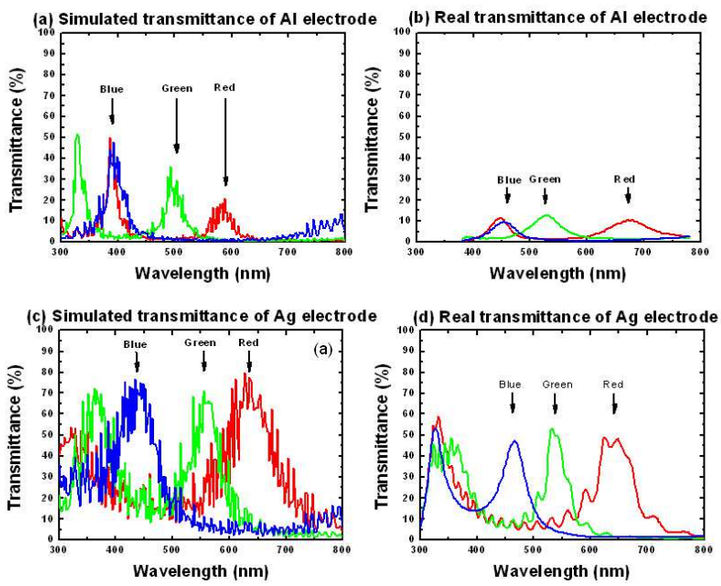

Fig. 29. Optical transmittance of different samples.

4.1.2 Color purity deviation

A color purity deviation (*CPD*) was defined in Equation 16 and was used to judge the color purity improvement in Figure 13. Figure 30 is the CIE chromaticity diagram for real devices

made with Al and Ag. As predicted by simulation in section 2.2, Ag samples showed better distribution for the three primary colors than Al samples did. Ag samples actually showed distinguishable red improvement, better blue, and comparable green. An averaged larger than 50% *CPD* refinement can be seen in red and blue colors. The *CPD* also implies that green color almost reached the target; blue color has little room to be improved; and red color still has great space to be refined.

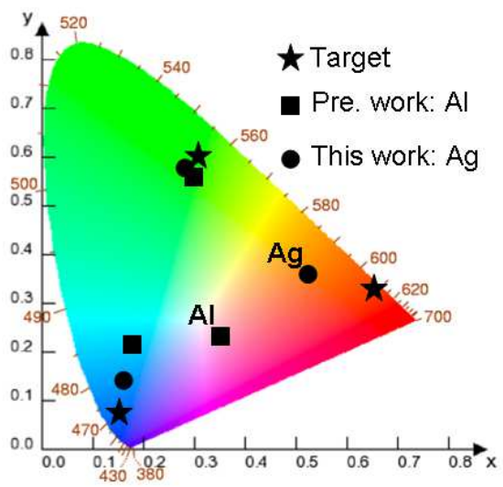

Fig. 30. Color purity comparison of previous and this works.

4.1.3 Transmittance

From Figure 29, around 20% transmittance difference was visible in both Al and Ag samples between simulation and real devices. This is believed to be the offset of simulation and real device. Besides the offset, as high as 40% unbalanced transmittance difference was in all Al colors but there is only less than 10% unbalanced transmittance difference in all Ag colors. Another important factor when judging the transmittance is its intensity. As shown in Figure 29(a)-(b), the intensities of all colors made by Al electrode are weak. This will become a serious perceptual issue if the substrate or extra protection layer absorbs some more intensity or when the backlight is weak. The common goal for all kinds of transmissive display device or color filter is to increase its transmittance intensity. In contrary, Ag samples showed higher intensity from both simulation and real device results.

4.1.4 Process variation induced color shift

The description in section 2.2 and the structure design implies that any variation of optical property and thickness of each layer will influence the output transmittance and color purity, it is important to understand how serious can these variation be. Table 3 is the simulation results for different Ag thicknesses. Since Ag was originally designed for 20nm and precise control was difficult, here a 25% (5nm) is set for the simulation. From the *CPD* point of view one may guess that 25nm should be the best setting for the smallest *CPD* for all colors. However, 5nm thickness lowered the highest transmittance peaks in red (618nm), green (562nm), and blue (426nm) for 7%, 15%, and 9%, respectively. Thus a 20nm Ag was finally decided as the process target. Table 4 is the simulation results for different isolation thicknesses, the variation is set to be ±40nm from each target. From the tables one can find

serious color shifts along all settings, which means that slight process difference will result in great color change. Since the isolation layer does not have transmittance issue, the thickness selection was made at the best locations for each color so that the smallest *CPD* also took place in these designs.

	Ag=15nm	Ag=20nm	Ag=25nm	Ag=30nm
Red SiO_2=160nm	0.26	0.21	0.16	0.13
Green SiO_2=325nm	0.22	0.17	0.12	0.09
Blue SiO_2=245nm	0.10	0.04	0.00	0.03

Table 3. C*PD* values with electrode layer (Ag) thickness skew.

Red	SiO_2=120nm	SiO_2=160nm	SiO_2=200nm
	0.39	0.21	0.40
Green	SiO_2=285nm	SiO_2=325nm	SiO_2=365nm
	0.34	0.17	0.35
Blue	SiO_2=200nm	SiO_2=245nm	SiO_2=285nm
	0.16	0.04	0.22

Table 4. C*PD* values with isolation layer (SiO_2) thickness skew.

The thickness variation of spacer layer was also performed and summarized in Table 5. Since there is no target value, no *CPD* calculation had been made. However, the data points represent the OFF state color output, thus how to keep these data points as close as possible to let OFF state color the same is very important. One simple way to check how close those data points are is to calculate the triangle area enclosed by those data points. The Heron's formula (or Hero's formula) describes the triangle's area (A_{OFF}) by its three lengths:

$$A_{OFF} = \sqrt{s(s-L_a)(s-L_b)(s-L_c)} \tag{27}$$

where

$$s = \frac{L_a + L_a + L_c}{2} \tag{28}$$

and

$$\begin{aligned} L_a &= \sqrt{(x_R - x_G)^2 + (y_R - y_G)^2} \\ L_b &= \sqrt{(x_G - x_B)^2 + (y_G - y_B)^2} \\ L_c &= \sqrt{(x_B - x_R)^2 + (y_B - y_R)^2} \end{aligned} \tag{29}$$

Here L_a, L_b, and L_c are the three lengths of a triangle; (x_R, y_R), (x_G, y_G), and (x_B, y_B) are the coordinates of each point. The smallest value of A_{OFF} happens on the 750nm spacer case within the three trials. Nevertheless, this spacer layer was gravure printing process prepared and its rheology characteristics have been plotted in Figure 27(c) which showed very limited linear region. In order to operate the gravure printing with sufficient process window, a compromised design of 600nm which located in the center of the linear rheology region was chosen.

	Spacer=450nm	Spacer=600nm	Spacer=750nm
Red SiO_2=160nm	(0.25, 0.22)	(0.30, 0.24)	(0.23, 0.25)
Green SiO_2=325nm	(0.30, 0.25)	(0.25, 0.26)	(0.22, 0.25)
Blue SiO_2=245nm	(0.22, 0.27)	(0.22, 0.26)	(0.28, 0.24)
A_{OFF}	0.001943	0.000300	0.000198

Table 5. CIE coordinates with spacer height skew.

4.2 Structural performance

4.2.1 Air channel

Even though the MEMS model also predicted several different solutions to lower the operation voltage with Equation 20, a better solution which avoids changing the device's vertical design was proposed in section 2.4. The introduction of air channel is believe to be helpful to reduce the air pressure trapped inside a single pixel when ON. As shown in Figure 31, the Newton's ring means the colorful interference part at the edge of an interferometer. The root cause of Newton's ring was the different optical interference path lengths (Γ). These different optical path lengths in turn represented different output interfered colors. An interesting behavior in the figure is that the Newton's ring's size neither increases linearly nor increases infinitely.

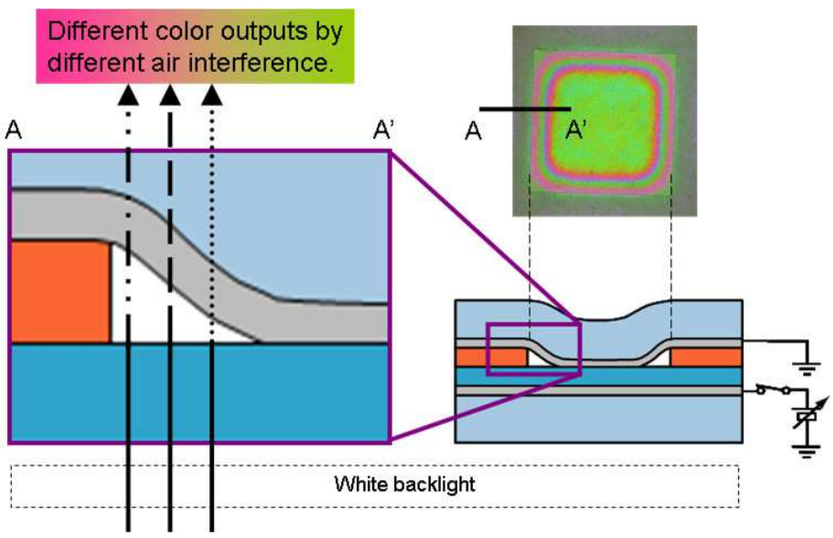

Fig. 31. A schematic plot to explain how Newton's ring took place.

Rather, the increment decreased along the increasing pixel size. A special saturation behavior of the Newton's ring's size appeared in Figure 32(a). This means that the increased pixel size will only make the display aperture looks larger instead of reduce the Newton's ring. This conclusion strongly supports the necessity of a revolutionary structure change. With different spacer coverage designs – 100% (no air channel), 90%, 80%, and 60% – the experimental data showed great amount of improvement. The width of Newton's ring reduced with all the coverage designs in Figure 32(b).

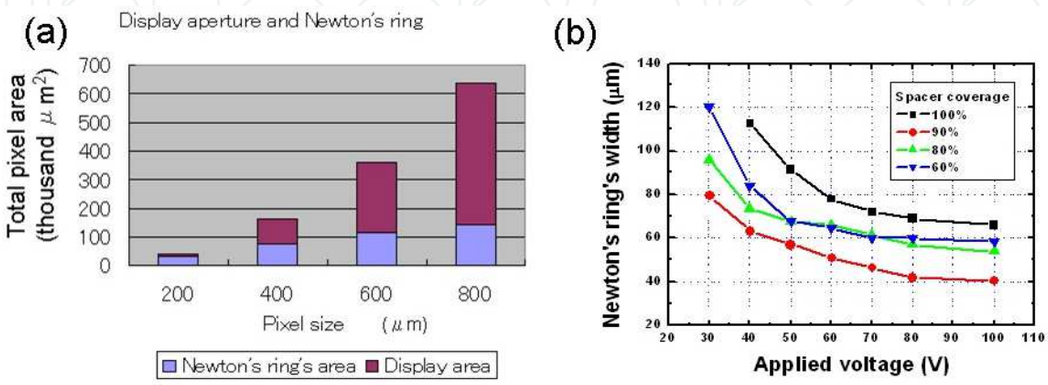

Fig. 32. Different spacer coverage alleviated the operation voltage.

Figure 33 is the picture which explains why saturation took place even with air channel design and why larger air channel did not yield in smaller Newton's ring: When the air channel is spacious enough, high applied voltage will let the lower layer attract the upper layer in the air channel area. Since the upper layer was put on the spacer and both sides (pixel area and air channel area) were competing each other, a see-saw performance showed – The more the air channel area in contact, the less the pixel area in contact. Thus a proper instead of a wide air channel is preferred. In this experiment a 90% coverage showed the smallest Newton's ring. This behavior was also obvious during simulation in Figure 20 and Figure 21: The display area tended to expand to the central part of air channel when the channel was wide enough but the display area tended to expand to the four corners when the channel with the same coverage was divided into two parts and were put aside. A combination of the experimental and simulation data suggested narrow and separate air channels are better. However, consider the resolution of printing process and the function of spacer layer for lamination, a single and large air channel was decided for the final structure.

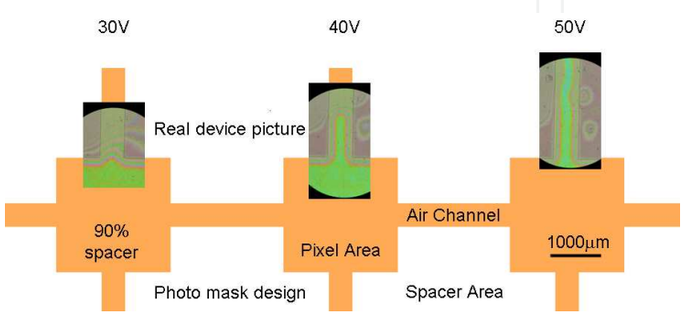

Fig. 33. Contact areas protruded into spacer areas when design was not optimized.

4.3 Electrical performance

4.3.1 Factors influencing electrical performance

The main target on the electrical performance of this MEMS display device is to reduce its operation voltage as described in the design part in section 2.3. However, to reduce the upper layer thickness together incorporate with the handling issue in which the electrostatic force is too strong on the <20μm PEN. The thin PEN will be easily attracted to the rubber pad and other equipment parts during printing and lamination processes by electrostatic force. The ultra thin upper layer will also induce special concerns on reliability. If extra layer should be added unto the whole structure, the transmittance and the optical performance should also be re-designed. Thus to reduce the thickness of the upper layer is not adequate.

	Spacer=400nm	Spacer=500nm	Spacer=600nm
Red SiO_2=160nm	(0.31, 0.21)	(0.19, 0.33)	(0.30, 0.24)
	0.10	0.12	0.07
Green SiO_2=325nm	(0.25, 0.24)	(0.25, 0.26)	(0.25, 0.26)
	0.09	0.08	0.08
Blue SiO_2=245nm	(0.19, 0.31)	(0.28, 0.24)	(0.22, 0.26)
	0.12	0.08	0.10

Table 6. *CPD* and its CIE coordinate under different spacer height settings.

To reduce the spacer height is not also a proper solution because the spacer height in OFF state also influences the output color as described in section 4.1. Table 6 is the list of simulated *CPD* under OFF state with white target of (0.31, 0.31) on CIE 1931 chromaticity diagram. The design goal not only fell on the small *CPD* but also required a small *CPD* difference between different colors. Both 400nm and 600nm spacer height designs are with smallest *CPD* differences $(0.10-0.07=0.12-0.09=0.03)$ but from the gravure printing characteristic point of view in Figure 27(c), the original 600nm design falls on the center part of the linear region thus provides more confidence on process control. Since the isolation layer thickness is the key for color interference, to reduce its thickness while keeping the same color design is then inaccessible. The final possibility fell on the pixel size and since this study aims on a large area display device for decoration, a 2000μm pixel size was set in section 2.3. Note that even though a 15V operation voltage was simulated in the same section, actual driving voltage was far higher than expectation in previous publication as listed in Table 7.

Pixel Size	Item	Red, SiO_2=370nm		Green, SiO_2=310nm		Blue, SiO_2=240nm	
		Sim.	Real	Sim.	Real	Sim.	Real
200μm	Voltage	65V	153V	55V	118V	40V	101V
	aperture	19%		19%		22%	
400μm	Voltage	40V	153V	30V	118V	28V	101V
	aperture	54%		54%		58%	
600μm	Voltage	34V	153V	25V	118V	22V	101V
	aperture	70%		68%		70%	
800μm	Voltage	28V	153V	25V	118V	18V	101V
	aperture	76%		78%		78%	

Table 7. Operation voltage difference between simulation and real device [35].

4.3.2 Combinational performance

Figure 34 is the three primary color pixels of the 3×3 MEMS flexible display demonstrator made partially by continuous and partially by discrete roll-to-roll printing processes operated under <20V. According to simulations, the contact area should be 93%(15V), 92%(20V), and 94%(20V) for red, green, and blue, respectively. These data typically match the expectations and the trend in Table 7. The big difference between these data and previous study is the Newton's ring's size. In the previous study the Newton's ring can be found under both small and large display apertures but the Newton's ring can merely be found in the green and blue pixel of this study because of the air channel design. This kind of improvements can be attributed to:

1. Low operation voltage – By using the air channel design to evacuate air pressure when ON;
2. Small Newton's ring – By replacing the steep spacer made by photolithography by the oblique ink spacer made by gravure printing.

The first merit was fully explained in section 4.2 and the second merit can be explained with Figure 35. Since the spacer structures were printed with pyramid shapes as shown in Figure 27(b), their oblique surfaces provide supports for the upper layer when ON. Also because of the black pigment doping in the spacer ink, the Newton's ring's color was blocked by the spacer structure.

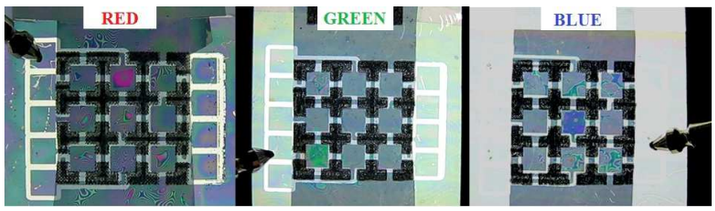

Fig. 34. The 3×3 test sample under ON state. A single pixel (square) is designed as 2000μm.

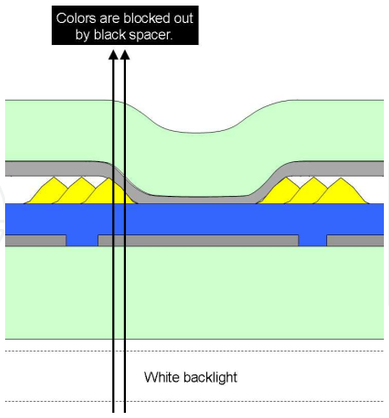

Fig. 35. A schematic plot to explain how Newton's ring was suppressed.

4.4 Yield performance

Section 4.1 to section 4.4 reviewed the MEMS flexible display device's characteristics. This section will review the roll-to-roll process's integrity from the mass production point of view.

4.4.1 Sheet to sheet uniformity

Figure 36 is the cumulative plot for electrode's sheet resistance (R_s). Since R_s excludes the influence by thickness, it represents a normalized impedance to its area with the following equation:

$$R_S = \frac{R \times w}{l} \tag{27}$$

where R is the sheet resitance. Note that the real line length (l) and real line width (w) will differ from the designed value, only the real value should be used to correlate with area size. Even though section 3.1 suggested a better flexography printing resolution along MD direction, electrical test revealed that the finest resolution was about 40μm for both transverse direction (TD) and MD. The data in this figure came from continuous 10m substrate with repeated 18 patterns for 8 times (sheets). The failure rate was 2.78% (4 out of 144) which is very compatible with current commercial semiconductor process lines. The whole patterning process done by the continuous roll-to-roll system including sacrificial ink printing, metal sputtering, and ultrasonic assisted lift-off was successfully developed and proved. From the figures we also understood that narrower lines were with larger standard deviations which implied poorer resolution controls. From the results, the smaller standard variation value of vertical patterns (0.54ohm/sq) also suggested better printing integrity along the MD direction. The TD patterns (whose standard variation is 0.85ohm/sq) showed finer lines but was by chance. Thus when one wants to try to obtain fine lines, it is suggested to design patterns normal (90°) to the printing direction but when one wants to obtain stable performance, it is suggested to design patterns along the printing direction. With these data, the developed lift-off process is suggested for the wider than 55μm line width applications.

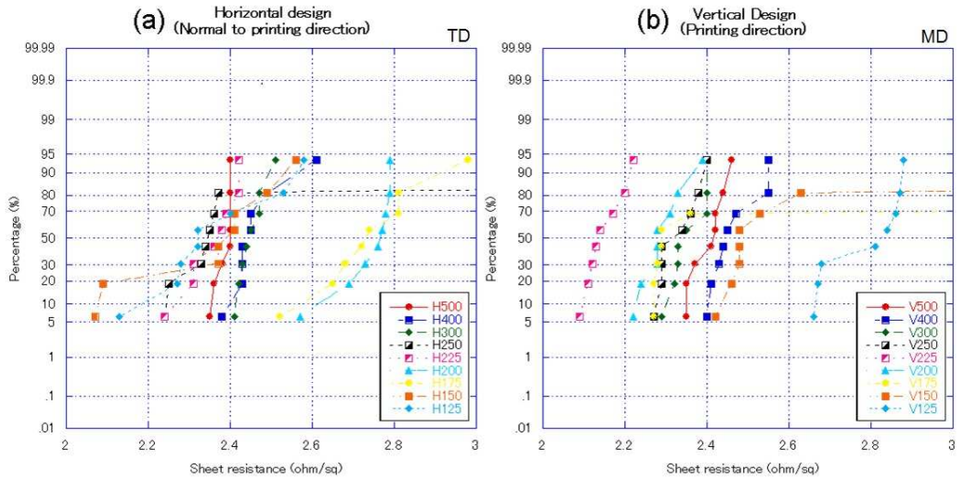

Fig. 36. Sheet resistance yield plots of electrode layer with (a) TD and (b) MD pattern.

4.4.2 Within sheet uniformity

Another test line set which occupies the whole sheet was used to check the within sheet uniformity. These test lines were designed only along the MD direction. Figure 37 is the cumulative plot for a 2mm long line which was used to fabricate passive matrix samples. Compared to Figure 36, these data were perfectly distributed with 100% as a sharp line since

the line width were relatively wider than the lines in the test pattern set, these 2mm lines were thus with less ink wetting induced variations from gravure printing. Even though the study goal is a large area MEMS controlled flexible display device, to develop a process which can support the requirement of the display system emerged parasitically. Thus this characterization section reviewed not only the device itself, but also the yield of the production line.

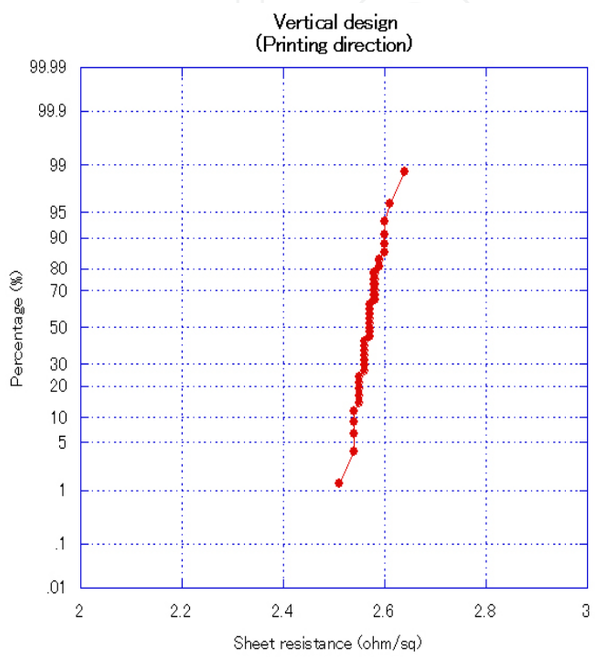

Fig. 37. Sheet resistance yield plots of electrode layer test patterns on the same sheet.

5. Summary and discussion

After review the micro MEMS display device's electrical, mechanical, and optical behaviors in previous section, this section will deal with some special considerations. These considerations came with the original design and sometimes worsened along the long term operation or the mass production. Thus the discussions on these considerations help on verifying some root causes of issues and also help on improving the device into a more complete design.

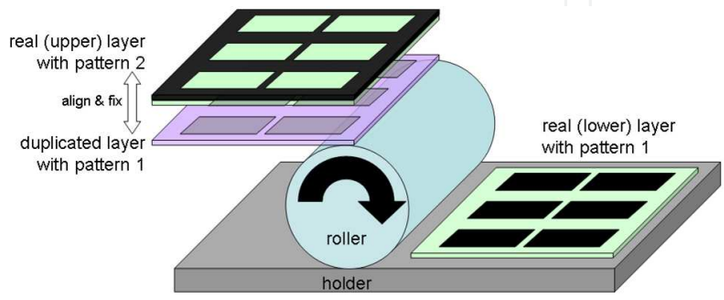

Fig. 38. The schematic plot for manual alignment and semi-auto lamination.

5.1 Alignment accuracy

This MEMS flexible display device was made partially by automatic continuous roll-to-roll system and partially by semi-auto discrete processes. Since the alignment apparatus was not yet installed in the roll-to-roll system shown in Figure 23, the alignment process during lamination of the two layers was performed manually. As shown in Figure 38, the lamination was performed with the test printer by the following procedures:

1. Prepare a duplicated lower layer pattern on a thin substrate,
2. Align the real upper layer with the duplicated layer and put them on the roller,
3. Put the real lower layer on the plate,
4. Activate the roller to laminate the two real layers,
5. Remove the dummy layer to obtain the laminated device.

The solution for misalignment is to install the lamination process into the continuous production line and control the same misalignment amount over a long distance. Figure 39 is the schematic plot for this idea. Let L_1>>L_2 and a is the smallest misalignment done by semi-auto system with manually alignment. Since the a value is fixed no matter how long the substrate is, when the process was aligned with a long substrate (L_1) and cut into smaller sheets (L_2) the misalignment amount b will be smaller than a. This kind of comparison was made base on the concept of unit length (here, the L_2). For example, the misalignment amount roughly reduced to 10% on the small area when the process distance was 10 times longer; the misalignment amount roughly reduced to 1% on the small area when the process distance was 100 times longer. When good alignment is expected on small areas, alignment mark can be added on both layers and registered and adjusted optically. Moreover, a feedback system which is capable to adjust the cylinder's location will also be helpful to adjust the alignment.

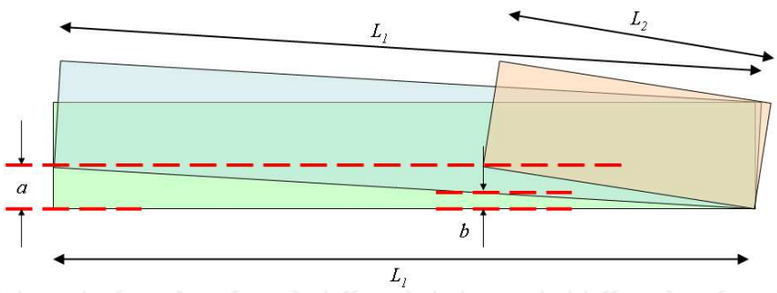

Fig. 39. The longer substrate helps on reducing the manual misalignment per unit length.

5.2 Color degradation

During the experiments and evaluations, a color degradation issue was found. The display color degraded from the original color after long term, high stress (voltage) operation. Note that the reliability test was cumulatively stressed from the low voltage → short term → long term → high voltage → short term → long term. Previous study attributed similar behavior to the reliability of thin electrode layer (12nm aluminum) and the strong electrostatic adhesion between upper electrode layer and the isolation layer. When they are in contact under stress, the upper electrode pealed off from the upper substrate and became incapable for color interference anymore. There was a light trend of display area with test sequence. This was because the isolation layer thickness difference and the charges started to accumulate from the thinnest areas. However, the charges were not smoothly removed

because the electric power was removed suddenly thus the display area did not 100% return to its original state. A study done with a periodical electric power supply which continuously switched between two polarities and thus the charges could be removed and the upper layer could return back to the original state. The electrodes with accumulated charges were further supported with more and more charges under the cumulative stress test, thus the display area expanded larger and larger. Some solutions for this reliability issue are thus proposed in three ways:

A. Solid isolation material

In order to obtain high and solid insulating material in a roll-to-roll process system, a sputter process is necessary and the sputter still matches the mass production requirement as the metal sputter process does. To continuously include the isolation layer sputter in the same apparatus of metal target can further reduce the process time (vacuum pumping) and the equipment space (add one target instead of add a machine).

B. Complete drying and curing process

Since the highest working temperature of plastic material is normally lower than 200°C, the over 350°C curing temperature for SiO_2 curing is not acceptable. This issue can be solved by replacing the plastic substrate by glass. Even though the glass substrate is fragile for shear stress, it can be made thin and thus flexible. Section 3.1 gave one example of how thin, how large, and how flexible can the thin glass be.

C. Doubled isolation layers

Either the sputtered SiO_2 or the completely cured SiO_2 ink will not solve the profound impact of electrostatic adhesion between upper electrode layer and the isolation layer. As a result, the sputtered SiO_2 or the completely cured SiO_2 ink will still degrade owing to the detachment of electrode material from the upper substrate. To prevent the electrode material from detaching from its substrate, a good solution is to cover the electrode with the isolation material. When this device is ON, the combinational thickness matches the color design value in the second section and the output color is expected to be the same. However, as summarized in Table 8, the OFF state non interfered color needs to be specially designed. The thickness in this table was easily divided the isolation layers into equivalent two parts from its originally designed value. Compared to the data for single layer, the data for double layer will form a larger triangle which is a drawback explained in section 4.1.

Structure	Isolation layer thickness (nm)	CIE coordinate when OFF	Difference
Single layer	Red=160	(0.30, 0.24)	---
	Green=325	(0.25, 0.26)	
	Blue=245	(0.22, 0.26)	
Double layer	Red=80×2	(0.32, 0.24)	acceptable
	Green=162×2	(0.29, 0.21)	acceptable
	Blue=122×2	(0.23, 0.44)	large

Table 8. OFF color difference from single and double layer designs.

5.3 Surface condition

Previously study concluded that the surface unevenness was the root cause for the poor color purity. The reference also concluded that the same issue caused the isolation breakdown. Furthermore, the surface unevenness structures distributed on the substrate surface mentioned in the reference were dense and uniformly spread on the substrate, the color interference of the defects then should not be as uniform as the data disclosed in the same reference. But even though the hypothesis was not correct, this surface defect should be eliminated. Figure 40 is the surface profile analyzed by atomic force microscope (AFM, SII NanoTechnology Inc., Nanopics). Here R_q is the root mean square value of measured data. The surface condition was monitored (a) before metal electrode sputtering, (b) after metal electrode sputtering, (c) after pattern lift-off, and (d) after isolation layer printing. There was no significant difference for the first three steps which suggested the substrate's profile was always inherited and followed from layer to layer until the SiO_2 was capped. Compared to the sputter and lift-off process, the gravure SiO_2 printing and the following drying and curing processes covered all these surface defects. The SiO_2 droplets transferred out from the gravure cylinder reflowed, spread, and finally merged before drying process provided a more uniform surface than the original substrate did. Thus the printing rheology is a key point for study.

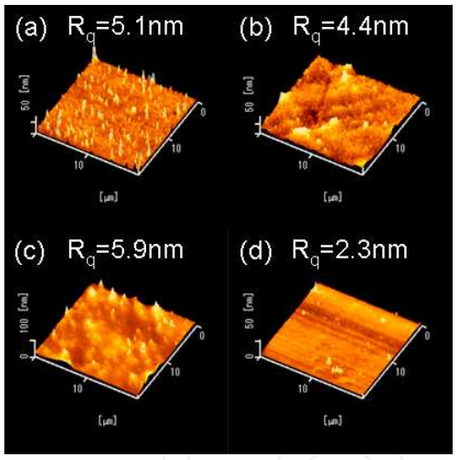

Fig. 40. Surface profile after different processes.

5.4 True colors

The purer red provided by Ag appeared owing to Ag's suitable optical parameters. However, the simulated and experimental data were not close to target red identified in Figure 13. Other metals such Au and Cu were examined to see how they provide interfered colors. Figure 41 is the simulations done with Au and Cu electrodes. As indicated by its color purity deviation (*CPD*), the red color by Au and green color by Cu provided smallest values. However, these values were not small enough to be true colors. Thus true colors of red and green require either new electrode materials or a multiple layer which serves as a single electrode layer to perform color interference. Other popular metals such as chrome (Cr) and cobalt (Co) were exempt from the simulation database because of their poor color and transmittance performance during simulation.

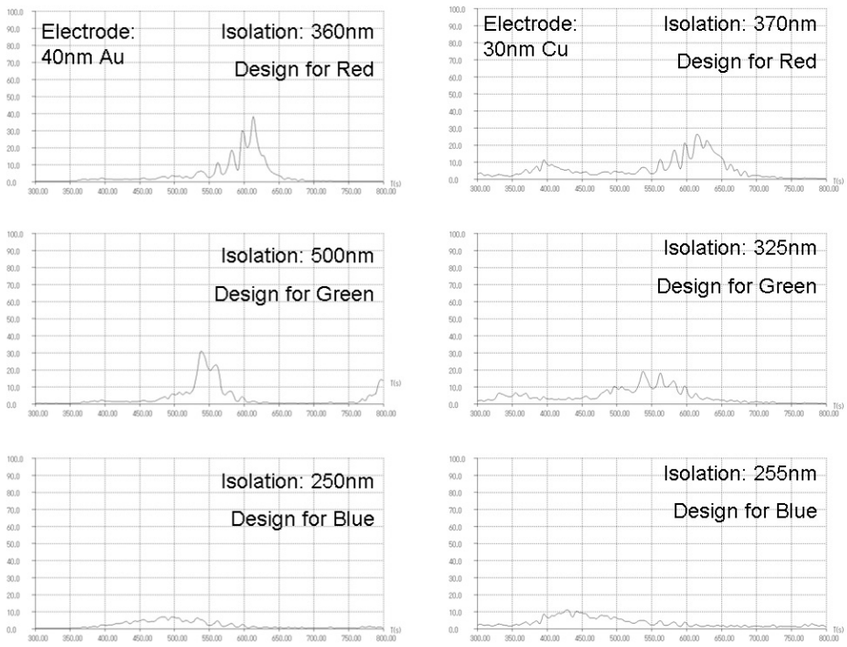

Fig. 41. Simulated best design with Au electrodes.

5.5 Structures

Even though the combinational full color display is not a must of the goal for decoration applications, this study implied a full color possibility by combining all three primary colors. However, the original design, which used a unified spacer thickness of 600nm, showed different combinational layer thickness. When combine the structures in Figure 11, a total thickness difference will appear since the isolation (Intermediate 5) thicknesses are different. This means that when using a unified lower substrate, the upper substrate will not be flat as shown in Figure 42. The uneven layer will not only cause process difficulties but will also result in reliability concerns. To overcome this, a structure with unified upper layer which requires different spacer heights and different isolation thickness for different colors should be designed. Some candidate solutions suggested in Table 9 provide uniform OFF state colors (same CIE coordinate). The process detail will be complicated but by doing this, the process issue disappears and the spacer heights can be controlled by gravure printing's cylinder and ink engineering discussed in section 3.4.

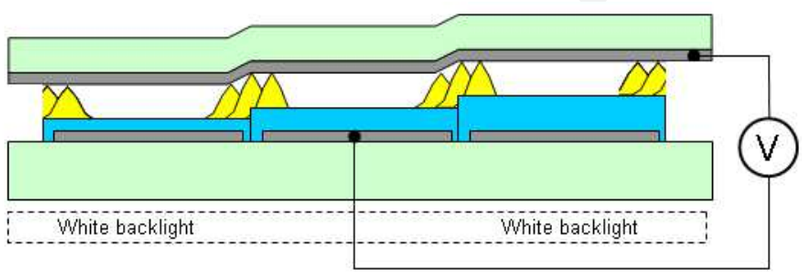

Fig. 42. Unified spacer height will leave an uneven upper layer.

	Solution 1		Solution 2		Solution 3	
	Spacer height (nm)	CIE coordinate when OFF	Spacer height (nm)	CIE coordinate when OFF	Spacer height (nm)	CIE coordinate when OFF
Red	765	(0.25, 0.26)	685	(0.22, 0.26)	600	(0.30, 0.24)
Green	600		520		445	
Blue	680		600		515	

Table 9. Color behavior under OFF states with uneven spacer heights

5.6 Processes

Recent research and development in the printed electronics field indicated usable Ag nano particle ink, which can be a good candidate for printed electrode. But designer also has to consider the influence of high resistivity of this ink because even though the resistivity does not influence the electrostatic behavior, the device requires a high electrical yield for connection lines. After these discussion focused on specific issues from process, material, and operation point of view with possible solutions, one can further expect a perfect final display device which is controlled by MEMS and manufactured by printing processes with flexibility.

6. Summary

The flexible MEMS by roll-to-roll printing system is an epoch-making concept that the system require neither solid substrate nor photolithography process.

A complex model which is a superposition of a single-end fixed cantilever and a parallel plate was proposed and proved by simulation and experiments. The model clearly indicated key parameters which play crucial roles on operation voltage which is also a key for portable, light weight, low cost, and maybe disaposable appliation. The Fabry-Perot color interferometer concept was taken as a demonstrator which was controlled by the MEMS. With this complex model, similar MEMS device can easily achieve low operation voltage which is a must for commercialization and safety concern.

The roll-to-roll process system showed a budget-friendly, high-efficiency, and large area supportive production and suggested high potential on replacing current photolithography technique for flexible applications.

With the successful electrical, mechanical, and optical demonstration, the large area flexible MEMS as well as the roll-to-roll printing process system opened great applications on portable and disposable electronic devices thus provided significant values in design and production fields.

7. Acknowledgment

The author wants to thank Prof. Dr. Hiroyuki Fujita and Prof. Dr. Hiroshi Toshiyoshi (both are with the University of Tokyo, Japan) for their advisory helps. The author also wants to thank Kuan-Hsun Liao, Sheng-An Kuo, and Chung-Yuan Yang for their lab works. The related works were partially supported by the following projects:

National Science Council (NSC) of Taiwan (Republic of China)

Research project (ID: 99-2218-E-007-018-MY2),
New Energy and Industrial Technology Development Organization (NEDO) of Japan
Industrial Technology Research Grant Program (ID: 06D48522d),
Japan Society for the Promotion of Science (JSPS)
International Training Program (ITP),
Finnish Funding Agency for Technology and Innovations (TEKES)
Funding decision 40104/07.

8. References

Abe, T., Yamashita, J., Shibata, H., Kato, Y., Matsumoto, H., & Iijama, T. (2008). *High-Accuracy Correction of Critical Dimension Errors Taking Sequence of Large-Scale Integrated Circuits Fabrication Processes into Account*, Journal of Micro-nanolithography MEMS and MOEMS, Vol. 7, Iss. 4, (October-December 2008), pp. 043008, ISSN 1932-5150

Author, G., & Martin, B. (1996). *Investigation of Photoresist-Specific Optical Proximity Effect*, Microelectronic Engineering, Vol. 30, Iss. 1-4, pp. 133-136, ISSN 0167-9317

Blanchet, G, B., Loo, Y., Rogers, J, A., Gao, F., & Fincher, C. R. (2003). *Large Area, High Resolution, Dry Printing of Conducting Polymers for Organic Electronics*, Applied Physics Letters, Vol. 82, No. 3, (January 2003), pp. 463-465, ISSN 0003-6951

Blanchet, G., & Rogers, J. (2003). *Printing Techniques for Plastic Electronics", Journal of Imaging Science and Technology*, Vol. 47, No. 4, (July-August 2003), pp. 296-303, ISSN 1062-3701

Boer, W, den. (2005). *Active Matrix Liquid Crystal Displays*, Elsevier Inc., ISBN 978-0-7506-7813-1, Burlington, USA

Bogacz, S., & Trafton, J, G. (2005). *Understanding Dynamic and Static Displays*, Cognitive Systems Research, Vol. 6, Iss. 4, (January 2005), pp. 312-319, ISSN 1389-0417

Corr, D., Bach, U., Fay, D., Kinsella, M., McAtamney, C., O'Reilly, F., Rao, S.N., & Stobie, N. (2003). *Coloured Electrochromic "Paper-quality" Displays Based on Modified Mesoporous Electrodes*, Solid State Ionics, Vol. 165, pp. 315-321, ISSN 0167-2738

Crawford, G, P. (2005). *Flexible Flat Panel Displays*, John Wiley & Sons, Ltd., ISBN 978-0-470-87048-8, Chichester, England

Crowley, J, M., Sheridon, N, K., & Romano, L. (2002). *Dipole Moments of Gyricon Balls*, Journal of Electrostatics, Vol. 55, pp. 247-259, ISSN 0304-3886

Cummins, D., Boschloo, G., Ryan, M., Corr, D., Rao, S, N., & Fitzmaurice, D. (2000). *Ultrafast Electrochromic Windows Based on Redox-chromophore Modified Nanostructured*, Journal of Physical Chemistry B, Vol. 104, pp. 11449-11459, ISSN 1520-6106

Hernandez, G. (1988). *Fabry-perot Interferometer*, Cambridge University Press, ISBN 0-521-36812-X, New York, USA

Ida, N. (2004). *Engineering Eletromagnetics*, Springer-verlag New York, LLC., ISBN 0-387-20156-4, New York, USA

Johnson, M, T., Zhou, G., Zehner, R., Amundson, K., Henzen, A., & Van de Kamer, J. (2006). *High-Quality Images on Electrophoretic Displays*, Journal of Society for Information Display, Vol. 14, Iss. 2, pp. 175-180, ISSN 1071-0922

Kim, J., Yang, K., Hong, S., & Lee, H. (2008). *Formation of Au Nano-patterns on Various Substrates Using Simplified Nano-Transfer Printing Method*, Applied Surface Science, Vol. 254, pp. 5607-5611, ISSN 0169-4332

Leech, P, W., & Lee, R. A. (2007). *Hot Embossing of Diffractive Optically Variable Images in Biaxially-Oriented Polypropylene*, Microelectronic Engineering, Vol. 84, pp. 25-30, ISSN 0167-9317

Lin, S, C., Lee, S, L., & Yang, C, L. (2009). *Spectral Filtering of Multiple Directly Modulated Channels for WDM Access Networks by Using an FP Etalon*, Journal of Optical Networking, Vol. 8, Iss. 3, (March 2009), pp. 308-316, ISSN 1943-0620

Lo, C., Huttunen, Hiitola-Keinänen, O. –H., Petäjä, J., Hast, J., Maaninen, A., Kopola, H., Fujita, H., & Toshiyoshi, H. (2008). *Active Matrix Flexible Display Array Fabricated by MEMS Printing Techniques*, Proceedings of The 15th Int. Display Workshop, pp. 1353-1356, Niigata, Japan, December 3-5, 2008

Lo, C., Huttunen, O, –H., Petäjä, J., Hast, J., Maaninen, A., Kopola, Fujita, H., & Toshiyoshi, H. (2007). *Novel Printing Processes for MEMS Fabry-perot Display Pixel*, Proceedings of The 14th Int. Display Workshop, pp. 1337-1340, ISBN 9781605603919, Sapporo, Japan, December 5-7, 2007

Marques, A., Moreno, I., Campos, J., & Yzuel, M, J. (2006). *Analysis of Fabry-Perot Interference Effects on The Modulation Properties of Liquid Crystal Displays*, Optics Communications, Vol. 265, Iss. 1, pp. 84-94, ISSN 0030-4018

Matsumoto, S. (1990). *Electronic Display Devices*, John Wiley & Sons, Inc., ISBN 0-471-92218-8, New York, USA

Obata, K., Sugioka, K., Shimazawa, N., & Midorikawa, K. (2006). *Fabrication of Microchip Based on UV Transparent Polymer for DNA Electrophoresis by F_2 Laser Ablation*, Applied physics A, Vol. 84, pp. 251-255, ISSN 0947-8396

Oh, H, –Y., Lee, C., & Lee, S. (2009). *Efficient Blue Organic Light-Emitting Diodes Using Newly-Developed Pyrene-Based Electron Transport Materials*, Organic Electronics, Vol. 10, Iss. 1, pp. 163-169, ISSN 1566-1199

Pollack, M, G., Fair, R, B., & Shenderov, A, D. (2000). *Electrowetting-based Actuation of Liquid Droplets for Microfluidic Applications*, Applied Physics Letters, Vol. 77, No. 11, (September 2000), pp. 1725-1726, ISSN 0003-6951

Puetz, J., & Aegerter, M. A. (2008). *Direct Gravure Printing of Indium Tin Oxide Nanoparticle Patterns on Polymer Foils*, Thin Solid Films, Vol. 561, pp. 4495-4501, ISSN 0040-6090

Schanda, J. (2007). *Colorimetry*, John Wiley & Sons, Inc., ISBN 978-0-470-04904-4, New Jersey, USA

Senda, K., Bae, B, S., & Esashi, M. (2008). *MEMS Membrane Switches Backplane for Matrix Driven Large Sign Display*, Proceedings of The 15th International Display Workshops, Vol. 2, pp. 1349-1352, Niigata, Japan, December 3-5, 2008

Senturia, S, D. (2001). *Microsystem Design*, Kluwer Academic Publishers, ISBN 0-306-47601-0, Massachusetts, USA

Smith, F, G. (2007). *Optics and Photonics*, John Wiley & Sons, Ltd., ISBN 978-0470017845, Chichester, England

Taii, Y. (2006). Master's degree thesis, The university of Tokyo

Taii, Y., Higo, A., Fujita, H., & Toshiyoshi, H. (2006). *A Transparent Sheet Display by Plastic MEMS*, Journal of Society for Information Display, Vol. 14, Iss. 8, pp. 735-741, ISSN 1071-0922

Vidotti, M., & Córdoba de Torresi, S, I. *(2008). Nanochromics: Old Materials, New Structures and Architectures for High Performance Devices*, Journal of the Brazilian *Chemical Society,* Vol. 19, No. 7, pp. 1248-1257, ISSN 0103-5053

Wang, Q, D., Duan, Y, G., Ding, Y. C., Lu, B. H., Xiang, J, W., & Yang, L. F. (2009). *Investigation on LIGA-like Process Based on Multilevel Imprint Lithography*, Microelectronics Journal, Vol. 40, Iss. 1, pp. 149-155, ISSN 0026-2692

Wong, W, S., Chabinyc, M. L., Limb, S., Ready, S, E., Lujan, R., Daniel, J., & Street, R, A. (2007). *Digital Lithographic Processing for Large-area Electronics*, Journal of Society for Information Display, Vol. 15, Iss. 7, pp. 463-470, ISSN 1071-0922

Acreo, http://www.acreo.se
Corning, http://www.corning.com
E Ink, http://www.eink.com
Ioffe Physical Technical Institute, http://www.ioffe.rssi.ru
Liquavista, http://www.liquavista.com/
Pixtronix, http://www.pixtronix.com
Qualcomm, http://www.qualcomm.com
Sipix, http://www.sipix.com
Silicon Light Machine, http://www.siliconlight.com
Texas Instruments, http://www.ti.com

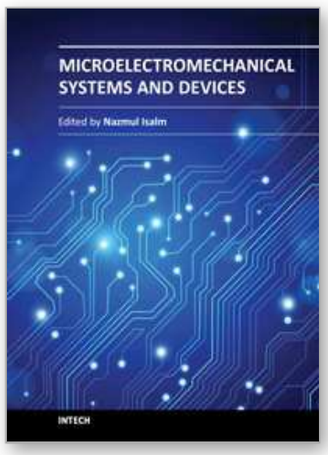

Microelectromechanical Systems and Devices

Edited by Dr Nazmul Islam

ISBN 978-953-51-0306-6
Hard cover, 480 pages
Publisher InTech
Published online 28, March, 2012
Published in print edition March, 2012

The advances of microelectromechanical systems (MEMS) and devices have been instrumental in the demonstration of new devices and applications, and even in the creation of new fields of research and development: bioMEMS, actuators, microfluidic devices, RF and optical MEMS. Experience indicates a need for MEMS book covering these materials as well as the most important process steps in bulk micro-machining and modeling. We are very pleased to present this book that contains 18 chapters, written by the experts in the field of MEMS. These chapters are groups into four broad sections of BioMEMS Devices, MEMS characterization and micromachining, RF and Optical MEMS, and MEMS based Actuators. The book starts with the emerging field of bioMEMS, including MEMS coil for retinal prostheses, DNA extraction by micro/bio-fluidics devices and acoustic biosensors. MEMS characterization, micromachining, macromodels, RF and Optical MEMS switches are discussed in next sections. The book concludes with the emphasis on MEMS based actuators.

INTECH
open science | open minds

InTech Europe
University Campus STeP Ri
Slavka Krautzeka 83/A
51000 Rijeka, Croatia
Phone: +385 (51) 770 447
Fax: +385 (51) 686 166
www.intechopen.com

InTech China
Unit 405, Office Block, Hotel Equatorial Shanghai
No.65, Yan An Road (West), Shanghai, 200040, China
中国上海市延安西路65号上海国际贵都大饭店办公楼405单元
Phone: +86-21-62489820
Fax: +86-21-62489821

IntechOpen